UNIVERSIDAD DE INVESTIGACIÓN DE TECNOLOGÍA EXPERIMENTAL YACHAY

Escuela de Ciencias Biológicas e Ingeniería

TÍTULO: Rapid detection of cardiac pathologies by neural networks using ECG signals (1D) and sECG images (3D): Exploratory study with 6-channel ECG.

Trabajo de integración curricular presentado como requisito para la obtención del título de **Ingeniero Biomédico**

Autor:

Aguiar Salazar Evelyn Dayana

Tutor:

PhD. Almeida Galárraga Diego Alfonso

Urcuquí, noviembre 2021

Urcuquí, 30 de noviembre de 2021

SECRETARÍA GENERAL
(Vicerrectorado Académico/Cancillería)
ESCUELA DE CIENCIAS BIOLÓGICAS E INGENIERÍA
CARRERA DE BIOMEDICINA
ACTA DE DEFENSA No. UITEY-BIO-2021-00036-AD

A los 30 días del mes de noviembre de 2021, a las 10:00 horas, de manera virtual mediante videoconferencia, y ante el Tribunal Calificador, integrado por los docentes:

Presidente Tribunal de Defensa	Mgs. VILLALBA MENESES, GANDHI FERNANDO
Miembro No Tutor	Dr. GUDIÑO GOMEZJURADO, MARCO ESTEBAN , Ph.D.
Tutor	Dr. ALMEIDA GALARRAGA, DIEGO ALFONSO , Ph.D.

El(la) señor(ita) estudiante **AGUIAR SALAZAR, EVELYN DAYANA**, con cédula de identidad No. **0604432120**, de la **ESCUELA DE CIENCIAS BIOLÓGICAS E INGENIERÍA**, de la Carrera de **BIOMEDICINA**, aprobada por el Consejo de Educación Superior (CES), mediante Resolución **RPC-SO-43-No.496-2014**, realiza a través de videoconferencia, la sustentación de su trabajo de titulación denominado: **Rapid detection of cardiac pathologies by neural networks using ECG signals (1D) and sECG images (3D): Exploratory study with 6-channel ECG**, previa a la obtención del título de **INGENIERO/A BIOMÉDICO/A**.

El citado trabajo de titulación, fue debidamente aprobado por el(los) docente(s):

Tutor	Dr. ALMEIDA GALARRAGA, DIEGO ALFONSO , Ph.D.

Y recibió las observaciones de los otros miembros del Tribunal Calificador, las mismas que han sido incorporadas por el(la) estudiante.

Previamente cumplidos los requisitos legales y reglamentarios, el trabajo de titulación fue sustentado por el(la) estudiante y examinado por los miembros del Tribunal Calificador. Escuchada la sustentación del trabajo de titulación a través de videoconferencia, que integró la exposición de el(la) estudiante sobre el contenido de la misma y las preguntas formuladas por los miembros del Tribunal, se califica la sustentación del trabajo de titulación con las siguientes calificaciones:

Tipo	Docente	Calificación
Tutor	Dr. ALMEIDA GALARRAGA, DIEGO ALFONSO , Ph.D.	10,0
Presidente Tribunal De Defensa	Mgs. VILLALBA MENESES, GANDHI FERNANDO	10,0
Miembro Tribunal De Defensa	Dr. GUDIÑO GOMEZJURADO, MARCO ESTEBAN , Ph.D.	10,0

Lo que da un promedio de: **10 (Diez punto Cero)**, sobre 10 (diez), equivalente a: **APROBADO**

Para constancia de lo actuado, firman los miembros del Tribunal Calificador, el/la estudiante y el/la secretario ad-hoc.

Certifico que *en cumplimiento del Decreto Ejecutivo 1017 de 16 de marzo de 2020, la defensa de trabajo de titulación (o examen de grado modalidad teórico práctica) se realizó vía virtual, por lo que las firmas de los miembros del Tribunal de Defensa de Grado, constan en forma digital.*

Firmado electrónicamente por:
EVELYN DAYANA AGUIAR SALAZAR

AGUIAR SALAZAR, EVELYN DAYANA
Estudiante

Firmado electrónicamente por:
GANDHI FERNANDO VILLALBA MENESES

Mgs. VILLALBA MENESES, GANDHI FERNANDO
Presidente Tribunal de Defensa

DIEGO ALFONSO ALMEIDA GALARRAGA
Firmado digitalmente por DIEGO ALFONSO ALMEIDA GALARRAGA
Fecha: 2021.11.30 16:44:35 -05'00'

Dr. ALMEIDA GALARRAGA, DIEGO ALFONSO , Ph.D.
Tutor

MARCO ESTEBAN GUDINO GOMEZJURADO

Firmado digitalmente por MARCO ESTEBAN GUDINO GOMEZJURADO
Fecha: 2021.12.01 08:48:28 -05'00'

Dr. GUDIÑO GOMEZJURADO, MARCO ESTEBAN , Ph.D.
Miembro No Tutor

Firmado electrónicamente por:
KARLA ESTEFANIA ALARCON FELIX

ALARCON FELIX, KARLA ESTEFANIA
Secretario Ad-hoc

Autoría

Yo, **Evelyn Dayana Aguiar Salazar**, con cédula de identidad 0604432120, declaro que las ideas, juicios, valoraciones, interpretaciones, consultas bibliográficas, definiciones y conceptualizaciones expuestas en el presente trabajo; así cómo, los procedimientos y herramientas utilizadas en la investigación, son de absoluta responsabilidad de el/la autora (a) del trabajo de integración curricular. Así mismo, me acojo a los reglamentos internos de la Universidad de Investigación de Tecnología Experimental Yachay.

Urcuquí, enero 2021.

Firmado electrónicamente por:
EVELYN DAYANA AGUIAR SALAZAR

Evelyn Dayana Aguiar Salazar

CI: 0604432120

Autorización de Publicación

Yo, **Evelyn Dayana Aguiar Salazar**, con cédula de identidad 0604432120, cedo a la Universidad de Investigación de Tecnología Experimental Yachay, los derechos de publicación de la presente obra, sin que deba haber un reconocimiento económico por este concepto. Declaro además que el texto del presente trabajo de titulación no podrá ser cedido a ninguna empresa editorial para su publicación u otros fines, sin contar previamente con la autorización escrita de la Universidad.

Asimismo, autorizo a la Universidad que realice la digitalización y publicación de este trabajo de integración curricular en el repositorio virtual, de conformidad a lo dispuesto en el Art. 144 de la Ley Orgánica de Educación Superior

Urcuquí, enero 2021.

Firmado electrónicamente por:
EVELYN DAYANA
AGUIAR SALAZAR

Evelyn Dayana Aguiar Salazar

CI: 0604432120

Dedication

This work is dedicated to my parents Luis and Patricia, my sister Mireya, my brother Sebastian, my brother-in-law Alexis, my beautiful four-legged son Max, and new puppy Nerón. They are the pillar and engine fundamental in my life. They always encouraged me to follow my dreams and to continue with my studies. In addition, they always supported me in the pleasures and adversities during all my life. They are my greatest treasure, and I will always be grateful to them.

In turn, I would like to dedicate this work to Diego Almeida to guide my academic formation and my inspiration to learn more. Besides being my teacher, he guided me to be a better professional and a better human being. Thank you for being my tutor, my mentor, and my friend.

Evelyn Aguiar Salazar

Acknowledgments

I want to express my deepest gratitude to my mother and brothers. They have encouraged and motivated me to achieve my goals and aspirations and have always supported me in every way possible to complete my degree. I especially want to thank my grandparents, Luis, Aida and Cleotilde, for being my strength and support to fulfil my dreams. Also, to my aunts, uncles, and cousins who have always been with me in one way or another.

I want to thank all my friends at Yachay, my second family. Especially to Diego S., Gaby O., Dianita L., Jeff S., Gaby P., Jona J., Michu S., Will S., Carli Q., Jean Pierre A., Mabe G., Bryan C., Edwin R., Andrecito P., Otto P., Juan Diego B., Dianita T., Erick C., Keila I., Mateo N., and Chris R. Thank you for giving me the best moments of my life and being my support. My university life was beautiful for each one of you. I will always carry you in my heart. Thanks for everything. Likewise, I want to thank my best friends Talia B. and Cristian Ch. Thank you for always giving me your support, and strength from a distance to keep going and never give up. Thanks for putting up with my temper. I am so lucky to have them in my life.

Also, I am immensely grateful to all the professors who trained me during my career, especially Diego A., Graciela S., and Fernando V. Also, to the School of Biological Sciences and Engineering and Yachay Tech University, where I received the best training, I could have had to be a professional of excellence. Finally, I thank the Biomedical Engineering Club for guiding me when choosing my career and for the good times, especially to my directive 2020-2021: Danny A., Mile Y., Leslie E., Jeff S., Anita A., Marle P., Nathy V., and Rosse D. Thank you for being more than my colleagues, being my friends, my support, and my confidants.

This thesis was written for the support of all of you. Thanks.

Evelyn Aguiar Salazar

"If we are not here tomorrow, let us be here today more than ever".

Resumen

Normalmente, la detección de patologías cardíacas se realiza mediante señales unidimensionales del electrocardiograma o con imágenes en 2D (bidimensionales). Cuando se trabaja con señales del electrocardiograma se puede representar en el dominio del tiempo y la frecuencia (señales en 1D). Sin embargo, esta técnica puede presentar dificultades como el elevado coste de los servicios sanitarios privados o el tiempo que tarda el sistema sanitario público en derivar al paciente al cardiólogo. Además, la variedad de patologías cardíacas (más de 20 tipos), es un problema en el diagnóstico de la enfermedad. Por otro lado, una de las técnicas poco exploradas para este diagnóstico es la electrocardiografía de superficie (sECG). Los sECG son imágenes en 3D (dos dimensiones en el espacio y una en el tiempo). En primer lugar, se construyó un electrocardiógrafo de 6 canales para registrar las señales precordiales del corazón. Posteriormente, se desarrollaron dos modelos, LSTM y ResNet34 NN, que mostraron una alta precisión, 98,71% y 93,64% respectivamente. Se realizaron mediciones en dos pacientes voluntarios en las que ambos modelos tuvieron éxito. El presente estudio propone las bases para el desarrollo de un software de ayuda a la decisión (DSS, por sus siglas en inglés) basado en modelos de aprendizaje automático.

Palabras clave: imágenes sECG, LSTM, ResNet34, redes neuronales, electrocardiógrafo 6-ch, Matlab, Python

Abstract

Normally, the detection of cardiac pathologies is performed using one-dimensional electrocardiogram signals or 2D (two-dimensional) images. When working with electrocardiogram signals, they can be represented in the time and frequency domain (1D signals). However, this technique can present difficulties, such as the high cost of private health services or the time taken by the public health system to refer the patient to a cardiologist. In addition, the variety of cardiac pathologies (more than 20 types) is a problem in the diagnosis of the disease. On the other hand, one of the little-explored techniques for this diagnosis is surface electrocardiography (sECG). sECGs are 3D images (two dimensions in space and one in time). First, a 6-channel electrocardiograph was built to record the precordial signals of the heart. Subsequently, two models, LSTM and ResNet34 NN, were developed and showed high accuracy, 98.71%, and 93.65%, respectively. Measurements were performed on two volunteer patients for which both models were successful. The present study proposes the basis for developing a Decision Support Software (DSS) based on machine learning models.

Keywords: sECG images, LSTM, ResNet34, Neural Networks, 6-channels electrocardiograph, MATLAB, Python

Contents

Anexes

List of Figures

List of Tables

List of Abbreviations

Acc: Accuracy

AF: Atrial Fibrillation.

ANN: Artificial Neural Networks

API: Application Programming Interface

AV: Atrioventricular Node

BN: Batch Normalization

BW: Bandwidth

CD: Conduction Disturbance

CNN: Convolutional Neural Network

Conv: Convolutional Layers

CSV: Comma-Separated Values File

DICOM-WS 30: Digital Imaging and Communication in Medicine Waveform Supplement

DP: Deep Learning

DSS: Decision Support Software

ECG: Electrocardiogram

F: Feature Map Dimension

FIS: Fuzzy Inference System

GPU: Graphics Processing Unit

H: Height Dimensions

HD: High-dimensional Computing (supervised ML algorithm)

HL7 aECG: Health Level Seven Annotated Electrocardiogram

HYP: Hypertrophy

ICD: Implantable Cardioverter Defibrillators

INEC: National Institute of Statistics and Census of Ecuador

K: Gain Filters

KNN: K Nearest Neighbor (supervised ML algorithm)

LSB: Least Significant Bit

LSTM: Long short-term Memory NN

MI: Myocardial Infarction

ML: Machine Learning

ms: milliseconds

MSN-Net: Multi-Scale Features-Concatenate Networks

MSP: Ministry of Public Health

NN: Neural Networks

N-Net: Multi-Lead Features-Concatenate Narrow Network

PAHO: Pan American Health Organization

PTB: Physikalisch-Technische Bundesanstalt

RAM: Random Access Memory

Rec: Recall

ReLu: Rectified Linear Unit

RNN: Recurrent Neural Network

SCP-ECG: Standard Communication Protocol for computer-assisted Electrocardiography

sECG: Surface Electrocardiogram

Spcf: Specificity

SQI: Signal Quality Index

STTC: ST/T Change

SN: Sinoatrial Node

TL: Transfer Learning

W: Width Dimensions

Wi: Filter Cutoff Frequency

WFDB: Wave Form Data Base

WHO: World Health Organization

Wo: Filter Central Frequency

Chapter 1: Introduction

1.1. Problem Statement

According to the World Health Organization (WHO), by 2030, almost 23.6 million people will die of heart disease, as heart disease is the leading cause of death globally, including heart disease and cerebrovascular disease [1]. Cardiovascular diseases are a group of disorders of the heart and blood vessels. They are classified as arterial hypertension, coronary heart disease, stroke, peripheral vascular disease, heart failure, rheumatic heart disease, congenital heart disease, and cardiomyopathies, and their respective types [1].

In Ecuador, cardiovascular diseases are the leading cause of death. In 2012, deaths from ischemic heart disease accounted for 10.3%, and cardiac arrests were reported for 7.7% of total deaths [2]. In 2014, the National Institute of Statistics and Census of Ecuador (INEC) reported 4430 deaths from ischemic heart disease, 1316 from heart failure, 168 from cardiac arrhythmias, and 106 from cardiac arrest [3].

In March 2016, the Pan American Health Organization (PAHO) conducted a survey in Ecuador on populations at risk for cardiovascular disease. The survey collected data from 2231 people between the ages of 18 and 69. This study showed that 30% of the population between 40 and 69 years of age is at risk of heart disease [4]. According to the 2018 STEPS survey, 25.8% of the population, aged 18 to 69 years, present three or more risk factors for chronic non-communicable diseases: high blood pressure, hyperglycemia, altered glucose, and high cholesterol [5]. Finally, according to the Ministry of Public Health (MSP), in 2019, 26.49% of the total number of deaths corresponded to heart disease [5].

Risk factors play an essential role in a person's likelihood of developing cardiovascular disease and are divided into two categories. On the one hand, the main factors are factors proven to play a role in the risk of cardiovascular disease: High blood pressure, high cholesterol, diabetes, obesity and overweight, smoking, physical inactivity, sex, heredity, and age [6]. On the other hand, secondary factors may or may not increase the risk of these diseases. These are stress, sex hormones, contraceptives, alcohol, and others. [6].

The more risk factors a person has, the more likely he or she is to suffer from heart disease.

The solution to all these problems is the constant monitoring of as many risk factors as possible to make the necessary lifestyle changes and medications to reduce cardiovascular risk. If so, a correct and timely diagnosis can prevent and help treat this type of disease. The critical element for the diagnosis of this type of disease is the use of an electrocardiograph.

1.2. Thesis Overview

This project is organized as follows: Chapter 1 includes the problem statement and the thesis overview. Followed by Chapter 2, which details the general and specific objectives of this study. Chapter 3 contains the essential concepts related to cardiac anatomy, physiology and pathologies, the fundaments of cardiac signals, and electrocardiographic leads. It also contains the characteristics of 1D, and 3D signals and the device used to detect them. This chapter ends with a description of the informatics fundaments used, as database and neural networks. Chapter 4 contains a detailed explanation of the methodology, which details the acquisition of the signal with its respective processing, the construction of the databases, and the predictive models. Chapter 5 contains the results obtained from signal and neural networks and the discussion of the present research compared with similar works. Finally, chapters 6 and 7 contain the conclusions reached and future perspectives for the work to continue.

Chapter 2:

Objectives and Hypothesis

2.1. Objetives

2.1.1. General Objective

To design two Neural Networks to compare ECG (1D) signals and sECG (3D) images to determine the best prediction tool for cardiac pathologies to prevent, monitor, and correctly apply rehabilitation to a patient.

2.1.2. Specific Objectives

- To store the signals in functional databases. The first database will be obtained from Pyshionet, and the second one will be built from the first one using MATLAB. Both databases will be divided into five categories.
- To build two predictive models: The first one, Long Short-Term Memory that will use as input the numerical values captured by clinical electrocardiographs, and the second one, Residual Neural Network that uses the sECG images as input.
- To determine the efficiency of both models by comparing evaluation metrics: specificity, sensitivity, and accuracy. After, the results will compare with previous studies related to the subject matter.
- To manufacture an electrocardiograph of 6 channels using electrode systems. This simple device can receive the six signals individually using Arduino.
- To obtain the signal and its prepossessing of two patients. For processing, the signals will be magnified, inverted, and filtered using the MATLAB program. To evaluate the results of two patients using the predictive models. They are to compare their efficacy when confronted with real cases.

2.2. Hypothesis

The Resnet34 neural network using sECG (3D) images presents better efficiency than the LSTM neural network using traditional ECG (1D) signals to diagnose cardiac pathologies.

Chapter 3:

State of the Art

3.1. Cardiac Anatomy and Physiology

The heart is a conical muscular organ. It is in the chest, and it tilts in this area, like an inverted triangle. The heart contains four chambers: two atria and two ventricles and four-valve: Tricuspid, Mitral, Aorta, and Pulmonic. The process of blood flow is the body's deoxygenated blood returns to the right atrium and then flows to the right ventricle. The right ventricle pumps blood into the lung, where it is oxidized. The blood then returns to the left atrium and flows to the left ventricle. Oxygenated blood is pumped from the left ventricle to the aorta and body.

3.1.1. Cardiac Cycle Dynamics

The cardiac cycle comprises all the physiological events associated with a single heartbeat, including electrical, mechanical, and heart sounds [7]. The cardiac cycle is split into two phases, systole (the contraction phase) and diastole (the relaxation phase). Each of these is then further divided into an atrial and ventricular component (Figure 1). The cardiac cycle proceeds in four stages:

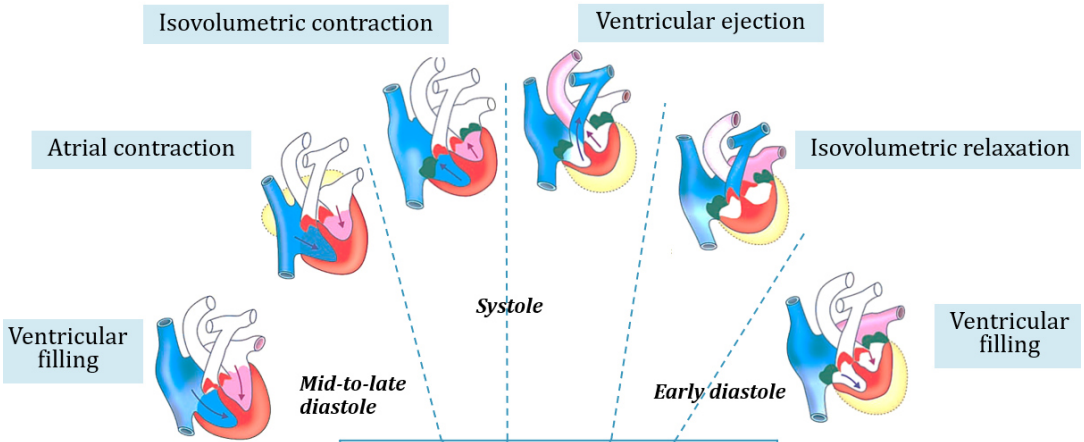

Phase	1	2	3	4	1
Atrioventricular valves	Open		Closed		Open
Aortic and pulmonary valves	Closed		Open		Closed

Figure 1. Cardiac cycle: atrial and ventricular component. Own elaboration from [7].

- **Atrial systole:** lasts about 0.1 seconds - both atria contract and force the blood from the atria into the ventricles [8].
- **Ventricular systole:** lasts about 0.3 seconds - ventricles contract, blood is forced to the lungs via the pulmonary trunk and the rest of the body via the aorta [8].
- **Atrial diastole:** lasting about 0.7 seconds - relaxation of the atria, during which the atria fill with blood from the large veins (the vena cava) [8].
- **Ventricular diastole:** lasts about 0.5 seconds - begins before atrial systole, allowing the ventricles to fill passively with blood from the atria [8].

3.1.2. Transmission of Electrical Impulses

Generation and transmission of electrical impulses depend on cell characteristics:

- **Automaticity:** a cell's ability to spontaneously initiate an impulse, such as found in pacemaker cells.
- **Excitability:** how well a cell responds to an electrical stimulus.
- **Conductivity:** the ability of a cell to transmit an electrical impulse to another cardiac cell.
- **Contractility:** how well the cell contracts after receiving a stimulus [8].

3.1.3. Depolarization- Repolarization Cycle

Cardiac cells undergo the following cycles of depolarization and repolarization as impulses are transmitted:

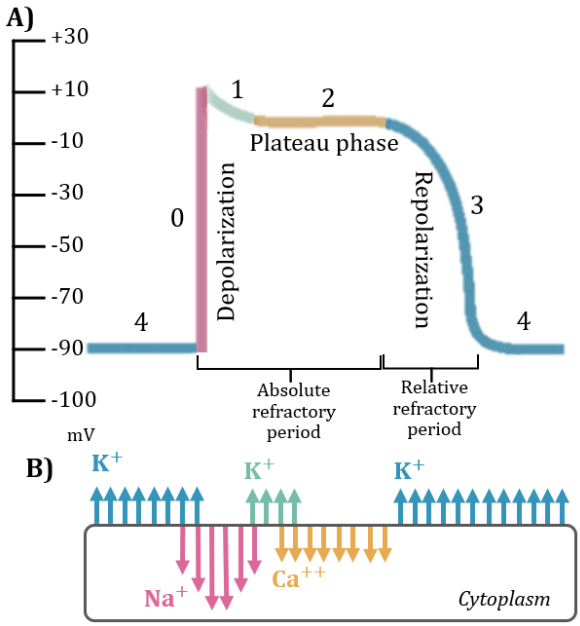

Figure 2. Action potential of myocardial contractile cells. A) Depolarization-repolarization cycle. B) Movements of ions through transmembrane ion channels. Own elaboration [9]

Phase 0: Rapid depolarization — the cell receives an impulse from a nearby cell and is depolarized.

Phase 1: Early repolarization — early rapid repolarization occurs.

Phase 2: Plateau phase — a period of slow repolarization occurs.

Phase 3: Rapid repolarization — the cell returns to its original state.

Phase 4: Resting phase — the cell rests and readies itself for another stimulus [7].

3.1.4. Cardiac Conduction System

After depolarization and repolarization occur, the resulting electrical impulse travels through the heart along a conduction system pathway. Impulses travel from the SA node and through the internodal tracts and Bachmann's bundle to the Atrioventricular (AV) node (Figure 3). From there, they travel through the bundle of His, the bundle branches, and lastly to the Purkinje fibers. Sinoatrial (SA) node generates 60 to 100 per minute; AV junction generates 40 to 60 per minute and Purkinje fibers of 20 to 40 impulses per minute [8].

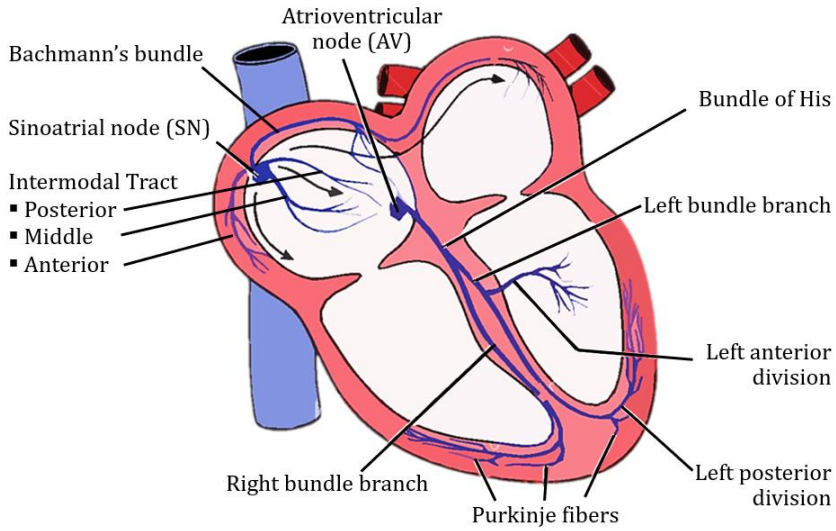

Figure 3. Elements of the cardiac conduction system. Own elaboration from [8].

3.2. Cardiac Signals

3.2.1. ECG Signals (1D)

The electrical signal produced by the heart is called an electrocardiogram (ECG). That is, it is the complex ECG represents electrical events that occur during the cardiac cycle [9]. These signals are traditionally used and are represented in the time domain or frequency (x-axis) and voltage (y-axis) [8]. ECG signals in 1D measurement in two dimensions: time and frequency domain. A complex wave consists of five waveforms marked with P, Q, R, S, and T (Figure 4). The waves Q, R, and S are called a unit, the QRS complex. The electrocardiogram depicts the

conduction of electrical impulses from the atria to the ventricles [7].

- **P wave:** Represents the depolarization of the atria. It has a rounded morphology, with a maximum duration of 0.10s (2.5 mm) and a voltage of 0.25 mV (2.5 mm). It is positive in all leads except in the frontal plane aVR, which is harmful, and in the horizontal plane lead V1 [8].
- **Q wave:** The initial negative deflection resulting from ventricular depolarization, which precedes an R wave. The duration of the Q wave is 0.010 - 0.020 sec [8].
- **R wave:** The first positive deflection during ventricular depolarization [8].
- **S wave:** The second negative deflection during ventricular depolarization [8].
- **T wave:** The slow deflection produced by ventricular repolarization[8].

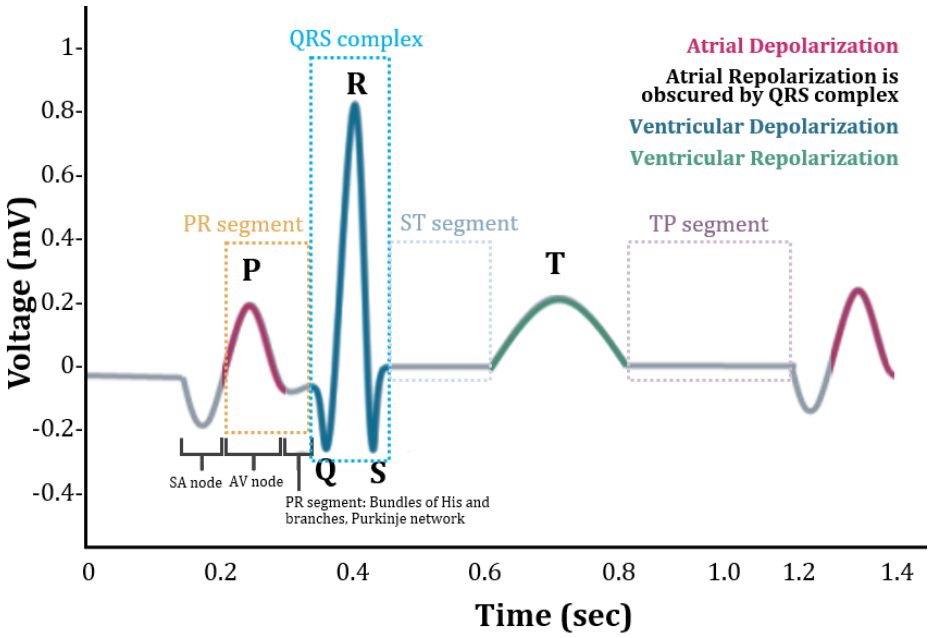

Figure 4. ECG complex. Own elaboration from [10].

Table 1. Characteristics of ECG signal [8], [11].

Amplitude (mV)	Frequency (Hz)	Bandwidth (Hz)	Types of electrodes	Measurement Error Source
1-5	0.1-300	0.05-100	Ag-AgCl disposable	Monitor artifact, 50/60 Hz powerline interference

3.2.2. sECG Images (3D)

One of the little-explored techniques for diagnosis is surface electrocardiography (sECG). The sECG are 3D images (two dimensions in space and one in time) constructed using frames which are divided into pixels corresponding to the electrodes whose signals, evolving in time, where each dashed line represents a square [12]. The colours are used to represent the instantaneous potential amplitude distribution, which is evolving [12].

This is a two-dimensional (2D) distribution of the instantaneous map of the surface potential (i.e., voltage) of the chest [13]. This potential distribution is an analogue (continuous) "electronic image" or "map" that evolves like a movie. The 2D analogue signal is sampled in space (through electrodes) and time (through electronic samplers) to provide a sequence of sampling time frames. In Figure 5, a frame is divided into pixels corresponding to the electrodes. The number of electrodes can vary from two (unipolar system) to hundreds. For example, high-density sECG (multichannel system) generates two-dimensional 3D sECG images in space and time [12] [14]. In this study, six channels were used to convert it into a 3D sECG. These concepts have been taken from sEMG studies and adapted to meet the stated objectives [12] [14][15][16][17].

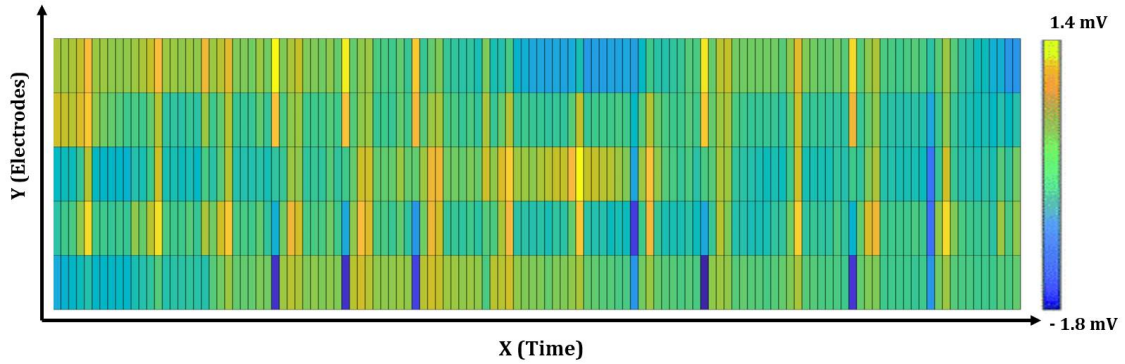

Figure 5. Example of sECG images.

3.3. Hardware Fundamentals

3.3.1. Electrocardiograph

It is clinical diagnostic equipment that captures and amplifies the electrical activity of the heart. Its operation is based on connecting a series of electrodes on the patient's skin in the thorax and extremities [9][18]. These electrodes allow capturing the electrical signal generated by the heart activity. The continuous recording of electrical impulses from the heart is called an electrocardiogram: this device detects heart problems and monitors the heart's health [8]. The structure of an electrocardiograph can be seen in the Figure 6.

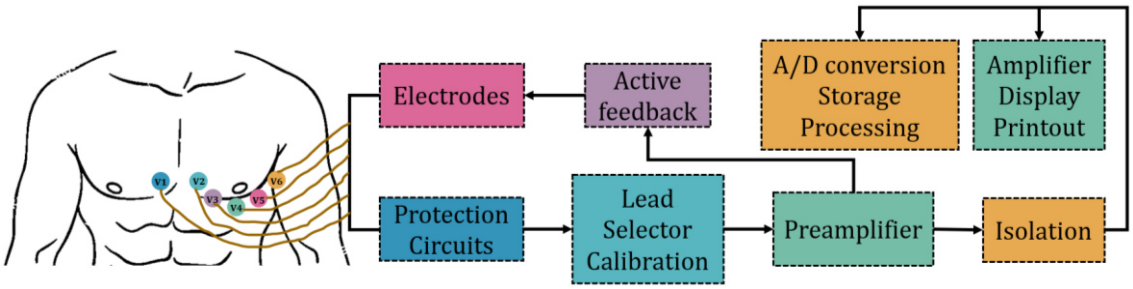

Figure 6. Block diagram of an electrocardiograph. Own elaboration from [19].

It consists of the following sections:

- **Protection circuits:** include surge limiters used in conjunction with defibrillators and may also include radiofrequency filters [19].
- **Lead Selector - Calibration:** Allows the leads to be recorded for programming. The calibration signal is a square wave pulse (amplitude=1mV). This signal generated that the amplitude of the input signal is compared with one of the known amplitudes [19].
- **Preamplifier:** In this stage, the signal obtained from the cable (DI-III) or the mean value of the rest (aVL, aVF, aVR, V1-6) is differentially amplified, relative to the isolation reference [19].
- **Active feedback:** this circuit is connected to the patient through the reference electrode and eliminates common-mode interference [19].
- **Isolation circuit:** the signal is transmitted between the isolation and network references [19].
- **Amplifier - Display - Printout:** The amplified signal can be displayed or printed on diagnostic paper [19].
- **A/D conversion - Storage – Processing:** digitizes the signal for storage or further processing [19].

3.3.2. Electrocardiographic Leads

Leads are specific electrode arrangements that record the potential difference generated by cardiac electrical activity at these points [9]. Electrocardiographic leads can be: Bipolar; they collect the potential difference between two electrodes located in specific body regions. Monopolar is the potential difference between an indifferent electrode with zero potential and an electrode located in a specific position [8]. The plane is divided into frontal plane shunts or limb shunts, with electrodes placed on upper and lower limbs. Horizontal plane leads or precordial leads, with their electrodes on the anterolateral chest wall [8].

Precordial leads provide information about the heart's horizontal plane and are monopolar. It is so, requiring only a single electrode. The opposing pole of those leads is the centre of the heart as calculated by the ECG (Figure 7). The precordial location of the electrodes is as follows: V1: the intersection of the suitable fourth intercostal space with the right border of the sternum. V2: the intersection of the 4th left intercostal space with the left border of the sternum. V3: midway between V2 and V4. V4: the intersection of the left fifth intercostal space and the mid-clavicular line. V5: the intersection of the left fifth intercostal space and anterior axillary line. V6: the intersection of the 5th left intercostal space and anterior axillary line [9].

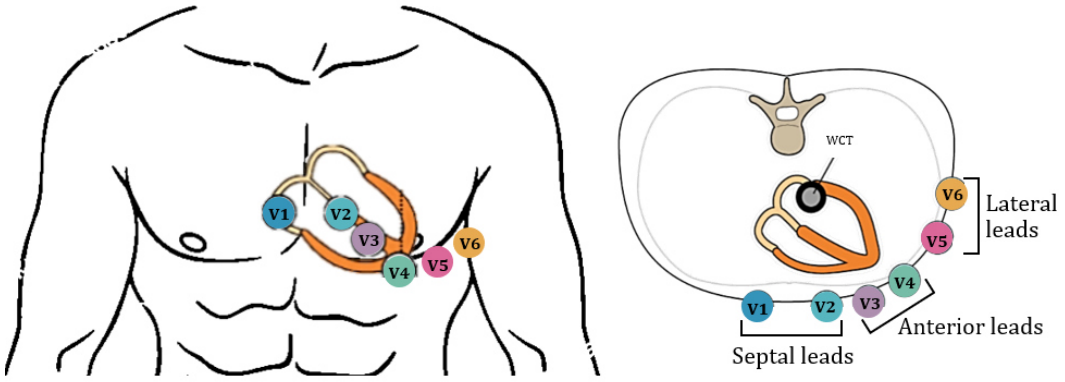

Figure 7. Precordial leads. WCT: Wilson central terminal, point centre of the thorax. Own elaboration from [9].

3.3.3. Types of Monitoring Electrocardiographs

The type of ECG monitoring system depends on the patient's condition and the location where the measurement is performed [8]. The two existing types are shown in Table 2.

Table 2. Comparison between Hardwire monitoring and Telemetry features [8].

Characteristics	Hardwire monitoring	Telemetry or Portable points
Electrode connection	directly from the patient using electrodes to the cardiac monitor via cables.	Directly from the patient, skin electrodes are connected by a thin cable to a transmitter box, which is in a pocket.
Location	permanently installed near the hospital bed.	Portable for use in medical operating rooms as they allow patient mobility.
Function	provides a continuous display of the heart rate and transmits the ECG trace to the console.	It is particularly useful for detecting arrhythmias that occur under-activity or stress.
Alarm	The monitor and console have alarms	Box and console have alarms
Other functions	record pulse oximetry, blood pressure, hemodynamic measurements, and other parameters.	None, they can only monitor heart rate and heart rhythm.
Disadvantages	Low patient movement Patient discomfort due to adherence of the electrodes and cables to the thorax. risk of disconnection and loss of the cable by the patient moves	It needs a constant change of batteries May suffer accidents such as falls

3.3.4. Commercial Devices

Electrocardiographs are essential devices in health centers for several reasons: It is the only diagnostic test that can assess cardiac electrical activity, it is a noninvasive diagnostic test, inexpensive and with immediate results, it is a very common procedure, and does not represent a large economic investment. When choosing an electrocardiograph, it is necessary to consider the technical elements and types available on the market. Among the characteristics that are important to consider are the type of technology (analog or digital), number of electrodes,

number of channels, thermosensitive paper or printing, and the adjustment options of the electrocardiograph. At present, electrocardiographs are commercial devices and come in different presentations. See Table 3 and Figure 8.

Table 3. Types of ECG commercial devices

ECG type	Users	State	Cost	Mechanism	Ref.
Bracelet	Athletes	Stress or movement	Low	Sensors	[20]
Chest belt	Athletes or people who need monitoring	Rest or movement	Medium	Electrodes	[21]
Portable monitors		Rest		Sensors	[22]
Clinical monitors	Medical personnel	Rest	High	Electrodes	[23]

(a) (b) (c) (d)

Figure 8. ECG types. A) Bracelet, B) Chest belt, C) Portable monitors, D) Clinical monitors. Own elaboration from [20]–[23]

3.3.5. Physical Components

For this research, three components were necessary. First, the Arduino Uno board is an open-source microcontroller board based on the ATmega328P microchip and developed by Arduino [24]. The board has 14 digital pins, six analogue pins and is programmable with the Arduino IDE via a USB type B cable. Second, ECG cables is a sensor cable with six ends located in the area for an electrode. These cables are 24 "long and have a male-male audio jack connector for the Arduino. It works with both 3.3 V and 5 V for boards, and its function is to establish a secure connection between the patient's electrodes and the electrocardiograph [25]. Third, Red Dot 3M electrodes are 6 cm in diameter and feature a patented solid gel that conforms to the skin quickly, allowing for high-quality, uninterrupted tracings. This gel contains low chloride content, which reduces skin irritation. The adhesives are sensitive to the patient's blood pressure and body warmth for optimal adherence [26].

3.4. Computer Fundamentals

3.4.1. Databases

It is an information repository that includes various forms of data on different topics and topics [27]. hey are data corresponding to the same content and are stored in an orderly manner for later use. Nowadays, due to technology development, the database has been developed in digital

computing [27]. Databases collect data such as addresses, names, characters, sequences, or multimedia files, such as videos, images, recordings, and others. These are stored systematically and are easy to be found.

3.4.2. Neural Networks (NN)

NN is a model inspired by the functions of the human brain, and its goal is to learn by automatically modifying itself so that it can perform complex tasks that cannot be classic rule-based programming can perform [28]. The NN receives a series of input values, and each of these inputs reaches a node called a neuron. Into layers that form a NN group the neurons sequentially. Each neurone in the network has a weight, a value, and it uses it to modify the input it receives [28]. It is so, obtains a new value that leaves the neuron and continues through the network. Once the network's end is reached, the output will be obtained, which will be the prediction calculated by the network [28]. Several types of NN models have the necessary characteristics depending on the database, the necessary outputs, the purpose of the network (prediction, recognition, and others), among many others. For the present study, the following types of NN will be defined:

3.4.2.1. Long Short- Term Memory Neural Networks (LSTM)

The LSTM is a recurrent neural network RNN that can learn long-term dependence [29]. In other words, it can remember information for a long time. All RNNs have the form of simple (1 layer) and repeating NN module chains. This chain structure is maintained in LSTM, but the repeating module consists of four layers [30]. LSTM can delete or add information to the cell state, carefully adjusted by the gate that optionally allows the information to pass through. They consist of a sigmoid NN layer and a dot product operation. The sigmoid layer describes when the component should be allowed to pass to generate a number between zero (no pass) and one (pass) [29][30]. LSTM has three such gates to protect and control the cell state.

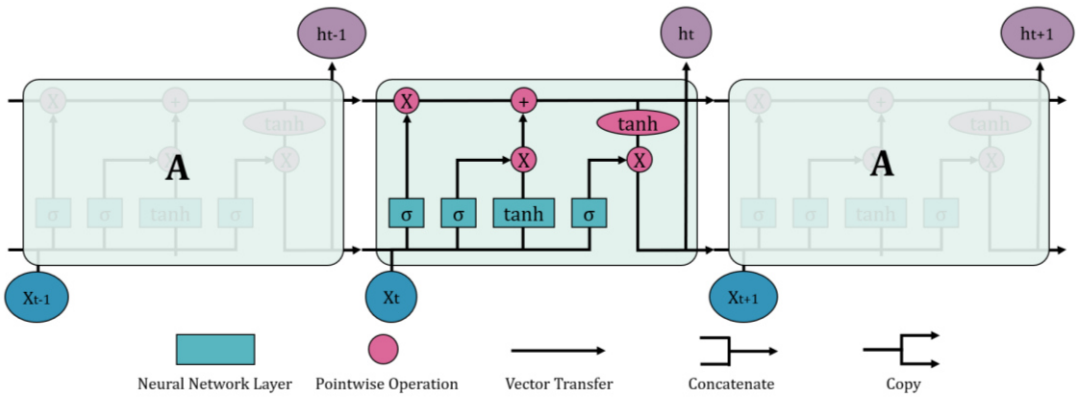

Figure 9. The internal structure of the LSTM layer. Own elaboration from [30]

To understand how LSTMs work, the process of Figure 9 is described: 1) Decide what information to remove from the cell state. This decision is made by a sigmoid layer called the "forgotten door layer". Here is a number between 0 and 1 for each number in the cell state: 1 means "keep this completely", and 0 means "get rid of this completely". 2) Decide what new information to store in the cell state. The second step has two parts: first, the sigmoid layer called the "gateway layer" determines which values will update. Next, the tanh layer creates a new candidate value vector which can be added to the state. 3) These two results are combined to create a status update. 4) It continues to update the previous cell state to the new cell state. For the old state, be multiply and add. These are new candidate values, which are scaled according to the degree of update of each state value. 5) The output will be based on the cell state but will be a filtered version. First, run a sigmoid layer to determine which parts of the cell state are generated. Then, it passes the unit state tanh (pushing the value between -1 and 1) and multiplies it by the output of the sigmoid gate to generate the part of interest [30].

3.4.2.2. ResNet34 Neural Networks

Resnet34 is a 34-layer convolutional neural network (CNN) used as an image classification model [31]. It is a model that has been pre-trained on the ImageNet dataset. However, it differs from traditional NN because it takes residuals from each layer and uses them in subsequent connection layers (similar to residual NN for text prediction). The residual building block for ResNet34 layers consists of multiple convolutional layers (Conv), batch normalization (BN), rectified linear unit (ReLU) activation functions, and shortcuts [32].

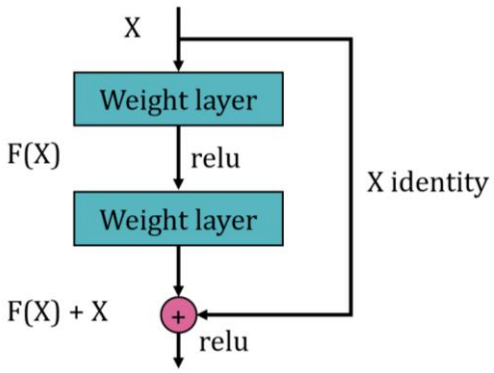

Figure 10. A "Basic-Block" building block for ResNet-34. Own elaboration from [32]

The output of the residual building block can be expressed as y=F(x)+x. Where F is the residual function, x is the input, and y is the output of the residual function [32]. The entire residual network consists of the first Conv and several basic blocks. The ResNet-34 contains 33 Conv, a max-pooling layer of size 3 × 3, an intermediate pool layer, followed by a fully connected layer [32]. A classical ResNet-34 model involves 63.5 million parameters, where rectification

nonlinearity (ReLU) activation and batch normalization (BN) is applied to the back of all convolution layers in the “Basic-Block” (Figure 10). In contrast, the SoftMax function is applied in the final layer [31].

Finally, the ResNet use the concept of Transfer Learning (TL). It consists in storing the knowledge acquired while solving a problem and applying it to a different but related problem. It is so, use the values of weights and biases of similar problems that have consumed a significant amount of time and computing resources in a new problem.

3.4.3. Computational Sources

For the development of this research, the use of the following computational sources was necessary:

3.4.3.1. Software and Programming Languages

Three software were used for the current project with their respective programming languages. The first was Collaboratory or Colab, a Google Research product that requires no configuration to use and provides free access to computing resources, including GPUs [33]. Colab used the Python programming language and interpreted, object-oriented, and high-level with dynamic semantics [34]. Python is simple syntax and easy to learn and supports modules and packages, encouraging program modularity and code reuse [34].

The second is MATLAB, numerical computing and programming platform used to analyze data, develop algorithms, and create models [35]. For the use of MATLAB, the M language was used, which is the software's language. This language works primarily with entire arrays and arrays. Its fundamental aspects include basic operations such as creating variables, indexing arrays, arithmetic operations, and data types [35].

The third is the Arduino software (IDE) that makes it easy to write code and upload it to the board [24]. Any Arduino board can use this software. The IDE is a set of software tools that allow programmers to develop and record all the code necessary to make the board work [36]. The Arduino IDE allows writing, debugging, editing, and recording programs or "sketches" effortlessly. Its programming language is based on C ++, the most accessible language to understand [24].

3.4.3.2. Python Frameworks and Libraries for Deep Learning (DP)

TensorFlow is an open-source library that performs numerical calculations using data flow diagrams. In other words, instead of coding a program, a graph is codified [37]. The nodes of this graph will be mathematical operations, and the edges represent the tensors

(multidimensional data matrices). Designing a graph increases the flexibility of execution [37]. Keras is a DP API, which runs on the TensorFlow machine learning platform [38]. It was developed to allow rapid experimentation. Keras uses other libraries (TensorFlow, CNTK, or Theano) transparently to do designated work. Its main features are: 1) It adopts the principle of progressive disclosure of complexity, and 2) it provides industrial-level performance and scalability [38].

fast.ai is a DP library that provides high-level components that quickly and easily result in standard DP domains [39]. Its layered architecture, which expresses common underlying patterns of DP and data processing techniques in terms of decoupled abstractions, does that ease of use, flexibility, and performance [39].

3.4.4. Digital Filters

A digital filter is a filter that operates on digital signals. It is a mathematical operation that takes a sequence of numbers (the input signal) and modifies it producing another sequence of numbers (the output signal) to highlight or attenuate specific characteristics [40]. Here was consider two:

A bandpass filter passes only signals whose frequencies are within a prescribed range (W1 <W <W2) [40]. The bandpass filter circuit combines a low pass filter and a high pass filter that will have a K gain over the required frequency range. Then, a band rejection filter lets through only the signals whose frequencies are outside a specific range (W1> W> W 2) [40]. The circuit is designed to set lower cutoff frequency 1 through the low pass filter, while the upper cutoff frequency W2 is set through the high pass filter. The frequency range between W1 and W2 is the filter bandwidth.

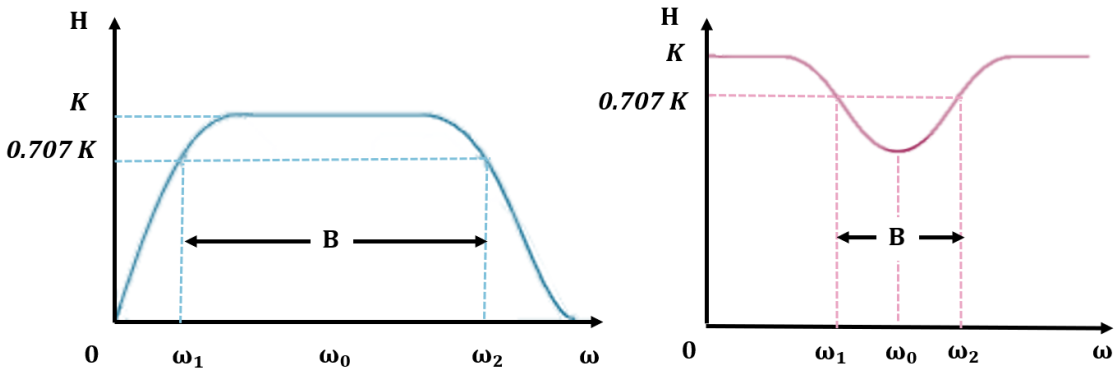

Figure 11. Frequency response of a) passband filter and b) band-reject filter. Own elaboration from [40].

3.5. Cardiac Pathologies

When the heart suffers a specific anatomical structure or physiology condition, it triggers a series of events that end with the development of cardiac pathology. These may be due to genetic factors, diet, sedentary life, among others [7]. Although there are more than 20 types [8], the following classes will be defined for this research:

3.5.1. Conduction Disturbance (CD)

CD is a problem in electronic systems; it makes the heartbeat and controls its rate and rhythm. In this type of disease, electrical signals cannot be generated correctly or pass through the heart correctly, or both. Certain drugs can cause CD. Diseases such as ischemic heart disease or myocardial infarction, or their genetics can also cause conduction disorders. CD can be treated with drugs, pacemakers, implantable cardioverter defibrillators (ICD), and surgery. Treatment depends on the location, type, and severity of the conduction disorder. The type of CD depends on its position in the conduction system. In this CD class are the following conditions: left anterior/left posterior fascicular block, incomplete right bundle branch block, incomplete left bundle branch block, complete left and/or right bundle branch block, AV block, non-specific intraventricular CD (block) and Wolf-Parkinson-White syndrome [41]. See the pathological changes at ECG in table 4.

3.5.2. Hypertrophy (HYP)

HYP is the increase in wall thickness due to the increase in the size of cardiomyocytes. Its cause is mechanical and neurohormonal stimulation and causes the heart to pump more blood. The thickened heart wall loses its elasticity, causing pressure to increase, filling the heart with the pump cavity and transporting blood to other parts of the body[42]. Many reasons can cause HYP, so many that it is not just cardiac HYP and the disease that causes it implicitly gives a prognosis; for example, a person with rheumatic fever or high blood pressure [7]. HYP usually develops gradually. People with HYP may have no signs or symptoms, especially in the early stages of the disease. As HYP progresses, they may experience shortness of breath, fatigue, chest pain, rapid heartbeat, violent beating (palpitations), and dizziness or fainting [8], [42]. In this HYP class are left and/or right ventricular hypertrophy, left and/or atrial right atrial overload/enlargement, and septal HYP [18]. See the pathological changes at ECG in table 4.

3.5.3. Myocardial Infarction (MI)

It is a type of ischemic cardiomyopathy, i.e., its cause is the deterioration or clogging of the heart's coronary arteries. Its cause can be the formation of plaques or clots of cholesterol, cells or lipids that cause total clogging of the arteries, resulting in the heart not being properly irrigated [7]. The cardiac cells in the affected area die due to the lack of blood circulation, causing irreversible damage to the patient. When this pathology occurs, time is a determining factor, so from the appearance of the first symptoms: pain in the chest and other areas of the body for more than 20 minutes, which does not disappear even with rest or deep breathing [9]. The realization of an electrocardiogram is a decisive test in these cases since it is the safest and fastest way to detect it [43]. This class of MI found the following conditions: anterior myocardial infarction, inferior myocardial infarction, lateral MI and posterior MI [41]. See the pathological changes at ECG in table 4.

3.5.4. ST/T Change (STTC)

The non-specific or strange T-wave and ST-segment changes on the ECG are because they do not expressly point to any medical conditions at all. Some changes in the ST segment or T wave of the ECG indicate specific conditions. These include ST-elevation MI, pericarditis, and hyperkalemia [44]. However, although a specific cause may cause these abnormalities, sometimes it is not the case, and there are only subtle abnormalities [8]. It is the same as the case of flat T wave, biphasic or asymmetric inversion. In the same way, the ST segment is dome-shaped, slightly depressed, or shows some elevation of the J point [44]. Sometimes, T wave and ST-segment changes are referred to as non-specific. While some severe forms of ECG are more classic and can help confirm the diagnosis, each condition is different. Pathologies in this class STTC include: ischemic in anterior leads, ischemic in inferior leads, non-specific ischemic, ST-T changes and non-specific ST changes [41]. See the pathological changes at ECG in table 4.

3.5.5. Characteristics Present in the Electrocardiogram

The electrocardiogram is usually used for the initial diagnosis of heart disease because it can detect the growth of the ventricles and changes in heart rhythm. The main characteristics of the pathology are described at Table 4.

Table 4. Characteristics present in the electrocardiogram of different pathologies.

	NORM	CD	HYP	MI	STTC
P wave	usually rounded and upright, and biphasic or variable in lead V1	-	in V1 is vast or mainly negative	-	-
Q wave	negative	-	-	pathologic wave in transmural myocardium	-
R wave	lead V5 large wave	-	high waves of V5-V6	-	-
S wave	lead V1 large negative wave	-	deep waves of V1 and V2	-	-
T wave	round and smooth. usually upright in leads V3 to V6; variable in all other precordial leads	-	negative waves	wave inversion	flat, oddly shaped or inverted
QRS complex	positive in leads V4 to V6 and negative in leads V1 to V3	-	100 ms and left bundle branch block	-	-
R-R interval	regular	variable intervals	-	-	-
ST-segment	usually isoelectric; may vary from	-	elevation	elevation	bulging, minimally depressed or shows some J-point elevation
Ref.	[8]	[45]	[46]	[43]	[44]

3.6. Related Works for Detection of Cardiac Pathologies using ECG (1D) and sECG (3D) signals.

First, there is a wide range of studies in which electrocardiographs have been developed, as shown in Table 5.

Table 5. Summary of the literature referring to ECG monitoring systems.

Signal acquisition	Signal preprocessing	Processing	Visualization	Type of leads	Ref.
X	X	X	X	3 channels Bipolar	[47], [48]
X		X		3 channels Bipolar	[49]
X	X	X		3 channels Bipolar	[50], [51]
X			X	12 channels Bipolar and Unipolar	[52]
X		X	X	32 channels ECG, EMG and PH level	[53]

This procedure starts with the acquisition of the patient's signal. It continues with the preprocessing that includes inverting and/or amplifying the signal. Next, processing includes signal filtering. Finally, visualization can be done graphically on a monitor. As can be seen, most of the investigations have been performed using three bipolar channels. On the other hand,

there are no records in which analyses have been performed using six unipolar channels. However, there are more complex electrocardiographs, such as 12 and 32 channels.

On the other hand, there are studies developed in software that detect cardiac pathologies, heartbeat detection, monitoring, motion detection, gesture recognition, and others. For this, artificial intelligence methods are generally used: machine learning and neural networks. First, studies using ECG signals (1D) have been used up to 15 channels from one channel. Secondly, no studies are using ECG signals (3D). However, there are studies on EMG signals (3D) using from 24 to 129 channels. All these aspects are shown in Table 6.

Table 6. Summary of the literature referring to ECG prediction models.

Type of AI	Application	Type of leads	Ref.
NN	ECG Heartbeat Classification	1 lead II ECG	[54]
NN	ECG Continuous monitoring	single channel ECG signal	[55], [56]
ML	Detection of MI	12 channels ECG Bipolar and Unipolar	[57]
NN	MI and Norm condition Classification	15 channels ECG Bipolar and Unipolar	[58]
ML	EMG signal of finger movements Detection	images sEMG of 24 channels	[59]
ML	EMG signal of finger movements Detection	images sEMG of 64 channels	[60]
NN	EMG Gesture recognition	images sEMG of 129 channels	[16]

** AI: Artificial intelligence, NN: Neural Network, ML: Machine Learning.

Chapter 4:

Methodology

The developed project in the present thesis has three parts: first, the NN was constructed using databases of numerical data and sECG images. Next, the NN architectures are presented and illustrated. Subsequently, the development of an exploratory study with a 6-channel electrocardiograph and its signal preprocessing methods. Finally, the performance verification of the models proposed through prediction in this research. Figure 12 shows the block diagram of the study. The goal is to build predictive models that can detect the occurrence of cardiac pathology by analyzing the 1D and 3D 6-lead ECG.

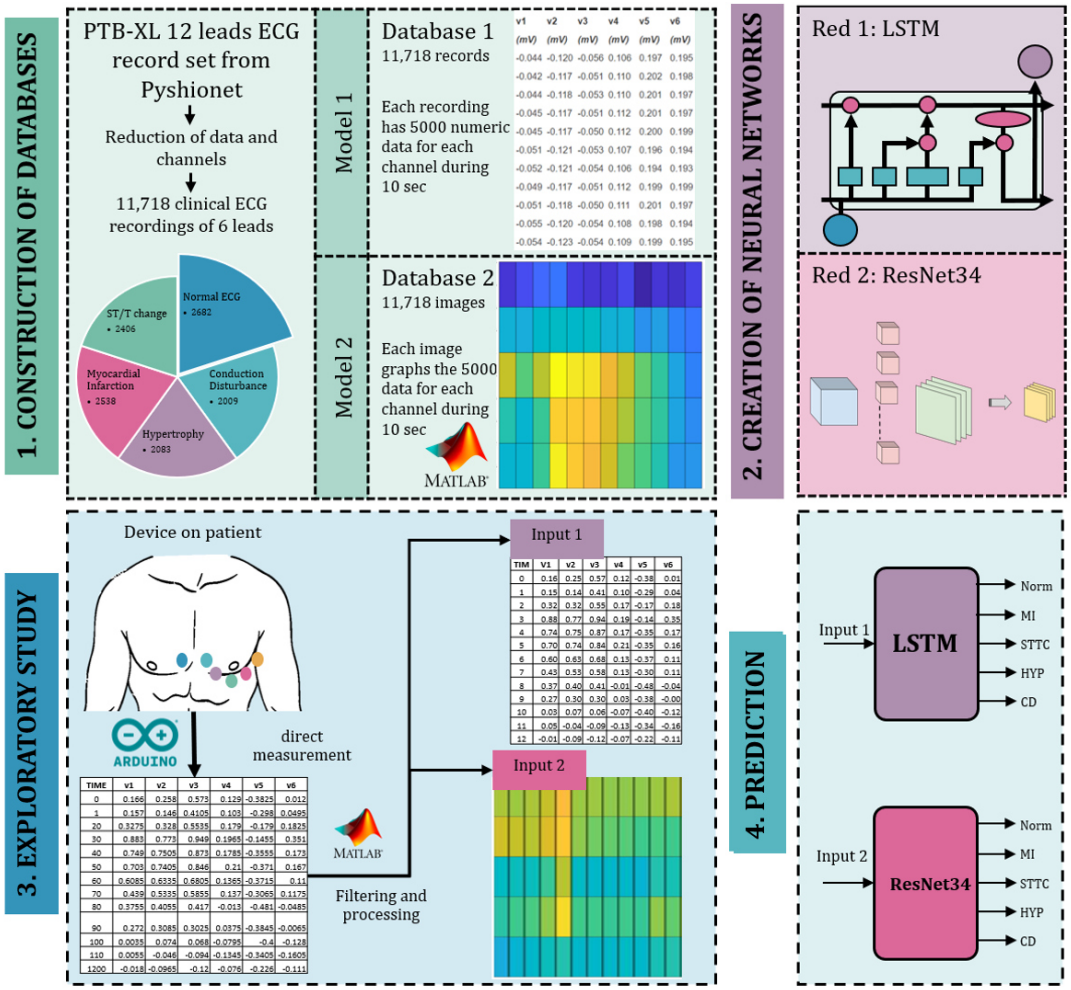

Figure 12. Block diagram of the research, including the signal processing, constructing the models, and the prediction final.

4.1. Databases

The PTB-XL ECG record set from Pyshionet [61] was used as an open-access database for this work. It is a set of 21837 clinical ECGs; each recording 12 leads to 18885 patients with 10 seconds [61]. The data were diagnosed by up to two cardiologists, who assigned additional features to each recording. The ECG recordings comply with the Standard Communication Protocol for computer-assisted Electrocardiography (SCP-ECG) [41]. It is a standard data format for ECG recording and defines the patient's ECG data structure, basic demographic format, and data exchange rules between digital ECG and computer systems [62]. It is the most recommended alternative to an ECG database.

A large amount of data makes this set a valuable resource for the training and evaluating automatic ECG interpretation algorithms. Additionally, the signals contain metadata on demographics, infarct characteristics, probabilities of diagnostic ECG statements, properties of annotated signals, and patient characteristics such as age, sex, weight, and others [41]; the present work metadata was not considered.

4.1.1. Database 1: Process of ECG Signals

For the present study, only the data of the precordial leads (V1, V2, V3, V4, V5, V6) were considered. In addition, the database contains 21837 records of cover diagnostic, form, and rhythm statements, for which only cover diagnostic records were considered. It is because the records of form and rhythm statements do not have the necessary characteristics for the objective of this research. With this data selection, the new database contains 11,718 records, distributed as shown in Table 7.

Table 7. SCP-ECG ID descriptions for classes and subclasses. Own elaboration from [41].

CLASSES			SUBCLASSES		
ID	Name	Records	ID	Name	Records
NORM	Normal ECG	2682	NORM	Normal ECG	2682
CD	Conduction Disturbance	2009	LAFB/LPFB	left anterior/left posterior fascicular block	247
			IRBBB	incomplete right bundle branch block	509
			ILBBB	incomplete left bundle branch block	16
			CLBBB	complete left bundle branch block	469
			CRBBB	complete right bundle branch block	237
			_AVB	AV block	295
			IVCB	non-specific intraventricular conduction disturbance (block)	162
			WPW	Wolff-Parkinson-White syndrome	74

HYP	Hypertrophy	2083	LVH	left ventricular hypertrophy	1718
			LAO/LAE	left atrial overload/enlargement	262
			RAO/RAE	right atrial overload/enlargement	77
			SEHYP	septal hypertrophy	26
MI	Myocardial Infarction	2538	AMI	anterior myocardial infarction	258
			IMI	inferior myocardial infarction	1678
			LMI	lateral myocardial infarction	570
			PMI	posterior myocardial infarction	32
STTC	ST/T change	2406	ISCA	ischemic in anterior leads	457
			ISCI	ischemic in inferior leads	287
			ISC_	non-specific ischemic	979
			STTC	ST-T changes	89
			NST_	non-specific ST changes	594

The database used classifies the data into five classes, each with its subclasses. This distribution of the dataset data is performed according to SCP-ECG standards and is represented graphically in Figure 13.

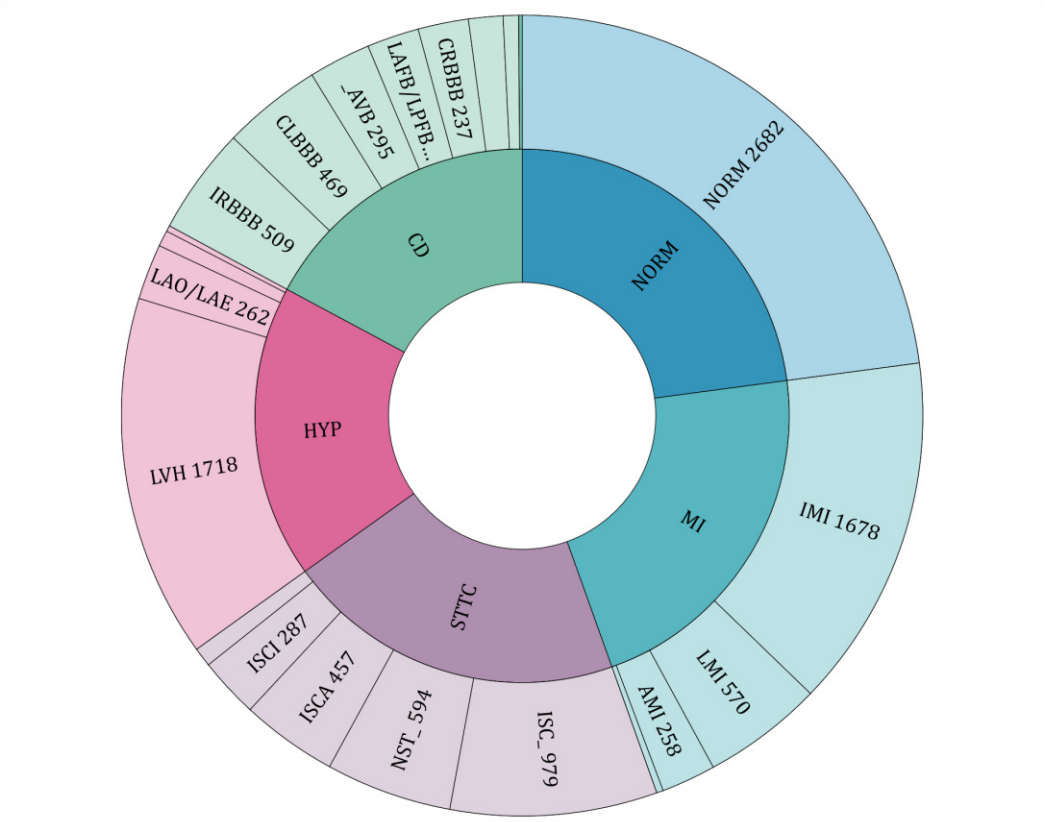

Figure 13. Graphical summary of the new dataset regarding diagnostic classes and subclasses, see Table 7. Own elaboration from [41].

The data set comprises 11,718 clinical ECG recordings of 6 leads of 10 seconds duration. These records were obtained from 10319 patients, of which 53.4% are male, and 46.6% are female, with ages ranging from 4 to 95 years (mean 56 and mode 65). The data set is a complete collection of several different concurrent pathologies and healthy control samples. The waveform files are stored in WaveForm DataBase (WFDB) format with 16-bit precision at a resolution of 1μV/LSB and a sampling rate of 500Hz. To see an example of the data, see Figure 14, considering that the measurements were for 10 seconds and 5000 samples.

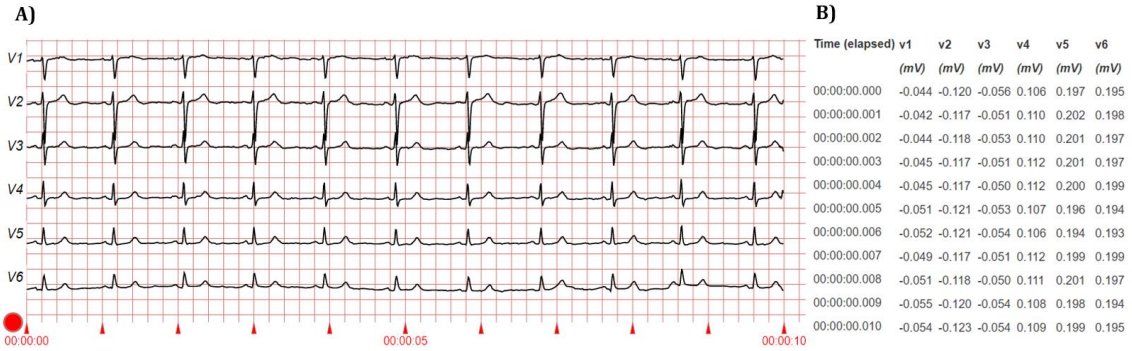

Time (elapsed)	v1 (mV)	v2 (mV)	v3 (mV)	v4 (mV)	v5 (mV)	v6 (mV)
00:00:00.000	-0.044	-0.120	-0.056	0.106	0.197	0.195
00:00:00.001	-0.042	-0.117	-0.051	0.110	0.202	0.198
00:00:00.002	-0.044	-0.118	-0.053	0.110	0.201	0.197
00:00:00.003	-0.045	-0.117	-0.051	0.112	0.201	0.197
00:00:00.004	-0.045	-0.117	-0.050	0.112	0.200	0.199
00:00:00.005	-0.051	-0.121	-0.053	0.107	0.196	0.194
00:00:00.006	-0.052	-0.121	-0.054	0.106	0.194	0.193
00:00:00.007	-0.049	-0.117	-0.051	0.112	0.199	0.199
00:00:00.008	-0.051	-0.118	-0.050	0.111	0.201	0.197
00:00:00.009	-0.055	-0.120	-0.054	0.108	0.198	0.194
00:00:00.010	-0.054	-0.123	-0.054	0.109	0.199	0.195

Figure 14. Example of patient 11275 with a diagnosis of MI A) Graph the ECG channels from V1 to V6 for 10 seconds. B) Values in mV of the ECG channels V1 to V6 during 10 microseconds. Own elaboration from [61].

4.1.2. Database 2: Construction of the sECG Images

For the construction of the sECGs, the entire database 1, i.e., the 11,718 recordings, was considered. First, all the WFDB files were converted to .xlsx format using Python functions, see Annex 1. Then each of the .xlsx files was passed through MATLAB using the function *[num,txt,raw] = xlsread (___)*. The variable x is defined as a vector corresponding to the number of measurements, and the variable Y is the number of channels. The function *[X, Y] = meshgrid (x, y)* is then used to transform the domain specified by the x and y vectors into X and Y matrices, to evaluate three-dimensional mesh and surface diagrams. The rows of the output matrix X are copies of the x vector; the columns of the output matrix Y are copies of the y vector. Then the matrix Z is defined as num, which is the numerical data of the .xlsx file. Finally, the mesh function is used to draw a mesh of wires with the colour determined by Z, so the colour is proportional to the surface height (voltage). That is, (X(j), Y(i), Z(i, j)) are the intersections of the grid lines of wires; X is the columns, and Y is the rows of Z. This resulting grid image is the surface ECG image, i.e., the sECG.

Table 8. Explanation of codes used in MATLAB for design sECG images.

Code	Explanation
`[num,txt,raw]= xlsread('1.Healthy1.xlsx')`	It returns three fields: the numeric data in an array, the text from the array of txt cells, and the text data from raw cells.
`x=0:0.080:9.92`	The vector from 0 to 10 seconds every 2 ms (0.002 seconds)
`y=1:1:6`	The vector from 1 to 6 representing V1, V2, V3, V4, V5, and V6.
`[X,Y]=meshgrid(x,y)`	Use of the meshgrid function to transform the x and y vectors into X and Y matrices.
`Z=num.'`	Z as the transposed num matrix
`mesh(X,Y,Z)`	Draw the mesh, where X and Y are the columns and rows of Z and Z is the value of the voltages represented by the color

The data set comprises 11,718 sECG images of 6 leads of 10 seconds duration that are designed using Database 1. In this plot, the value in the matrix represents the z-value in the plot. The dimensions of the matrix base on the x and y values are based.

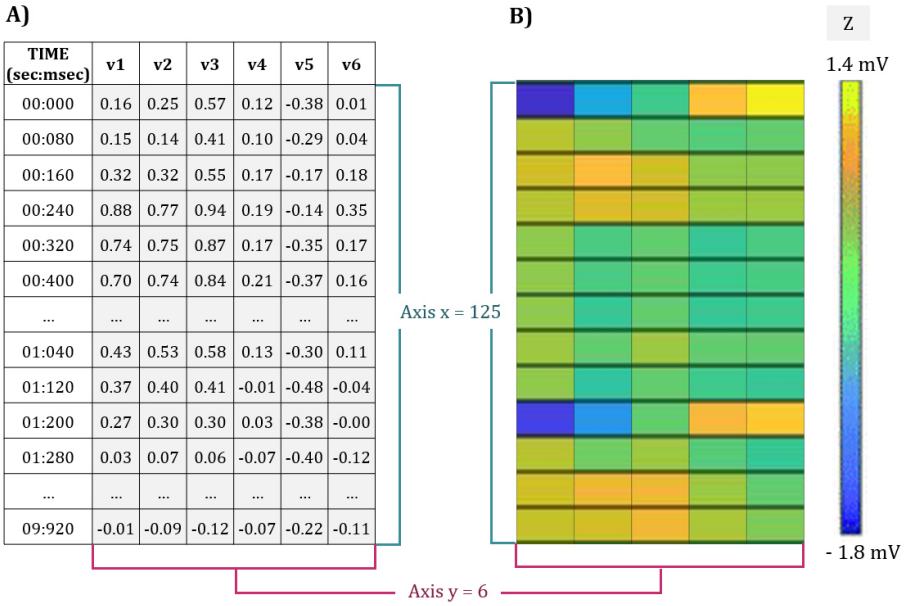

Figure 15. Explanation of sECG image formation. A) Example of 125 numerical data, records taken every 80 ms. B) Representation of the sECG image.

4.2. Neural Networks

The models were built in Google Colab in Python language. GPU and the High RAM function were used because of the large amount of data to train. Both had the 11718 records divided into training and validation. The construction of 2 models is described below: Model 1 (LSTM) works with cardiac signals (1D) and model 2 (ResNet34) works with sECG images (3D).

4.2.1. Computational Analysis: LSTM NN

For this model imported several libraries:

- *wdfb* and *tqdm* for reading and processing the WDFB files
- *os* for reading the files in the various directions
- *math* and *matplotlib* for the mathematical and graphical calculations
- *keras* and *sklearn* for the construction and learning of the model
- *numpy*, *pandas*, and *time* for various actions

Then, read the WDFB files with the conditions mentioned in section 4.1.1 and distribute the training and validation datasets. To construct a Sequential model is necessarily planed a stack of layers where each layer has exactly one input tensor and one output tensor. To this was construed the function *make_model* that permits add the layers used to *add()* method. The model has three types of layers: LSTM, Dropout, and Dense. The coupling of the layers was performed with a fixed feature map dimension (F) [256, 128, 64, 32, 5]. Also, other resources were used, such as optimizers, dropouts, and activation functions mentioned later.

Subsequently, although the parameters of each of the classes are balanced in quantity, an adjustment of weights was made [63]. It is to match the values obtained by the network for each of the classes. The model was designed with the *make_model* function mentioned above using the lengths of the train set (values) as input, the length of the train set (labels) as output, and the LSTM layer as the leading layer of the model. To see the code used, see Annex 2. To see the model's architecture, see figure 16, which shows the order of the layers and the number of values that entered and exited each one of them. Here are mentioned several hyperparameters that will be described later.

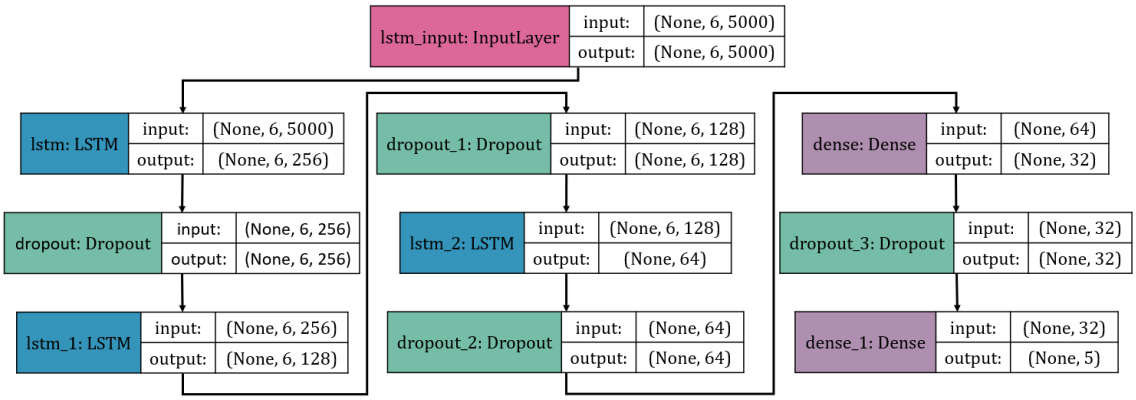

Figure 16. LSTM Network architecture and parameters at each layer

4.2.2. Computational Analysis: ResNet34 NN

For this model, start by importing the last version of the fastai repository and all the required libraries. Then, read the *WDFB* files with the conditions mentioned in section 4.1.1 and distribute the training and validation datasets. Now load the images in a *DataBlock* object. It allows to load the images directly from the folders, load the images with the exact sizes, define the images per batch, and identify the ones used for training, validation, and test. Also, it makes the transformations required. Also, it makes the transformations required. Then this object pass to the *DataLoader* function that provides a simplified and consistent Application Programming Interface (API) via batching and caching [64]. As mentioned in section 3.4.2.2, this network uses the concept of TL. So, a pre-trained model was used through the *cnn_learner* function. Here are mentioned several hyperparameters that will be described later. To see the code used, see Annex 3.

To see the model's architecture, see figure 17, which shows the order of the layers and the number of values that entered and exited each one of them. ResNet34 consists of one convolution and pooling step followed by four layers of similar behavior. Each of the layers follows the same pattern. They perform 3x3 convolution with a fixed feature map dimension (F) [64, 128, 256, 512] respectively, bypassing the input every two convolutions.

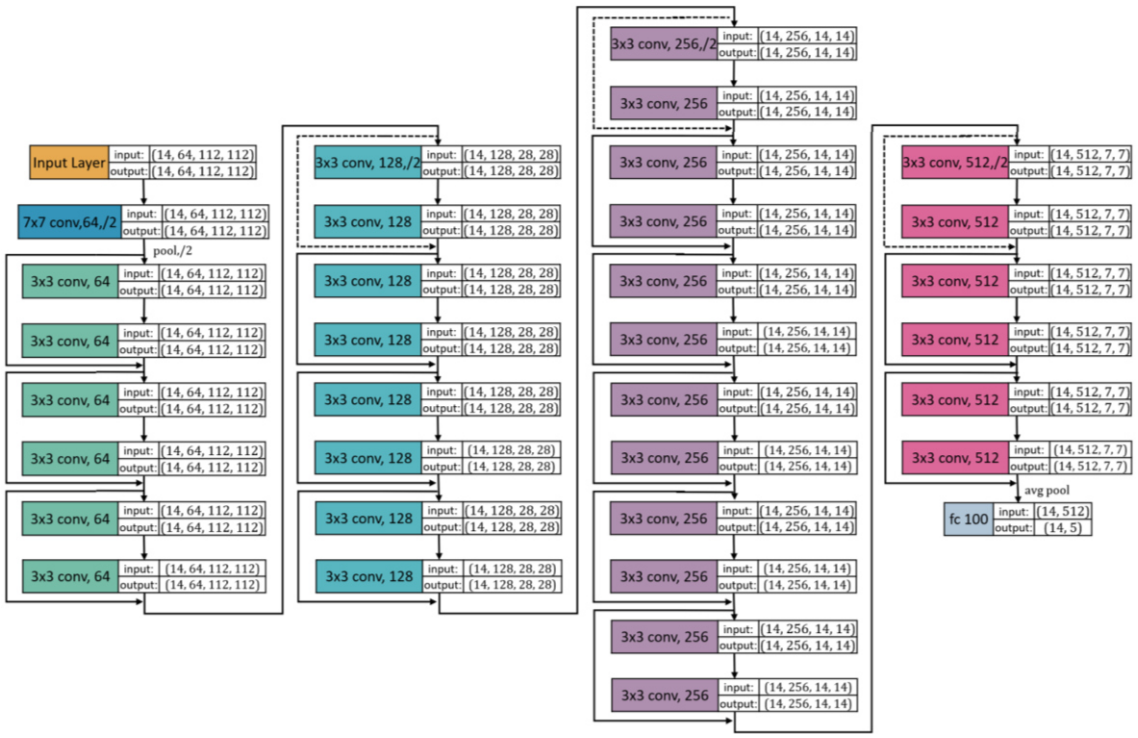

Figure 17. ResNet34 Network architecture and parameters at each layer

Furthermore, the width (W) and height (H) dimensions remain constant during the entire layer. The dotted line shows a change in the dimension of the input volume (a reduction because of the convolution). The reduction between layers is by an increase in stride, from 1 to 2, at the first convolution of each layer.

4.3. Exploratory Study with a 6-channel Electrocardiograph

Two steps were followed to exploratory study:

- Electrocardiograph using electrode systems
- Processing the signal with MATLAB

4.3.1. Electrocardiograph using Electrode Systems

For the construction of the 6-channel Electrocardiograph, was used an Arduino Uno board, 6 ECG signal cables, and Red Dot 3m electrodes. These three parts were assembled simply by connecting the wires to the analogue ports of the board (Figure 18). This analogue system oversees capturing the signal to process it later digitally. Physiological signals are continuous and can take any amplitude value, that is, infinite decimal places. Therefore, the best way is also to capture them in an analogue way.

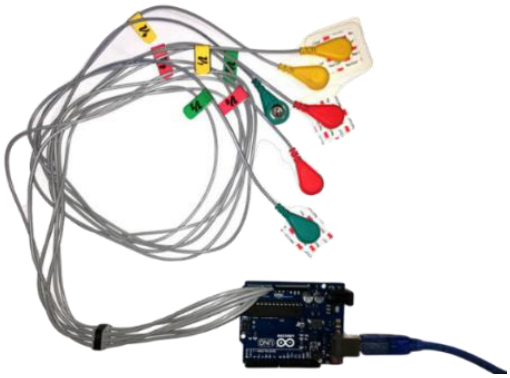

Figure 18. Construction of the 6-Channel Electrocardiograph

A clinical electrocardiograph can process 12 leads simultaneously, while commercial electrocardiographs usually work with three leads. The current project used six precordial leads. To process of measurement of ECG signals, first must inform the patient of the procedure to be performed; it is painless and does not exist a risk of damage. Second, should undress the patient's chest and place the patient in the supine position. Then, to put the six precordial electrodes will follow the steps (Figure 19).

V1 is placed in the fourth intercostal space, just on the right edge of the sternum. **V2** is placed in the fourth intercostal space, just the left edge of the sternum. **V4** is placed in the fifth

intercostal space, on the midclavicular line, which is the line that descends vertically from the mid clavicle. **V3** is placed in the intermediate position between electrodes V2 and V4. **V5** is placed on the same line as V4 but on the anterior axillary line, which is a vertical line between the center of the clavicle and its outer end. Finally, **V6** is placed on the same horizontal line as V4 and V5 but on the mid-axillary line, which is a line that runs vertically from the center of the armpit.

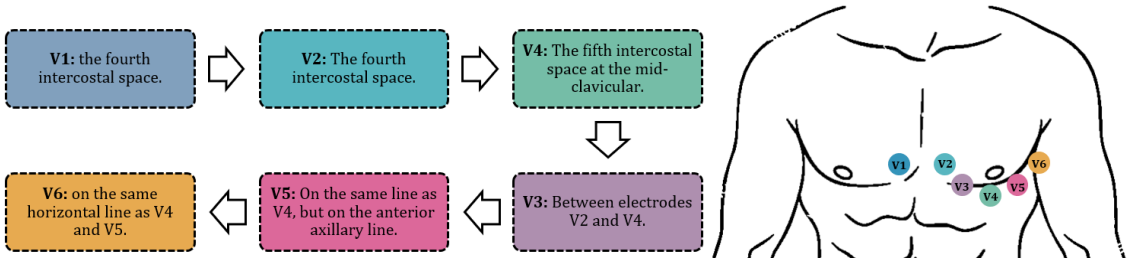

Figure 19. Description of the location of the precordial electrodes in the human body

For the present investigation, as a sample taken two volunteer patients. Following the protocol, they were measured with the electrocardiograph. Table 9 found the characteristics of the two patients. Both patients were selected according to their cardiac condition of healthy and sick, which will allow a comparative study of both neural networks. According to the prediction made, it will be possible to compare with the reality that each patient presents at present.

Table 9. Characteristics of the patients used for the study.

ID	Age	Sex	Height (cm)	Weight (kg)	Cardiac history	Observations
Patient01	20	Male	172	68.5	No antecedents	Apparently normal subject
Patient02	32	Male	164	72.5	Two months ago, he suffered a MI	He has heart failure

At this point, the Arduino Uno board is ideal as it has six analogue inputs. In addition, due to the processing speed of the Arduino Uno, it can only do one task at a time. It must sample each channel separately, one after the other, making it ideal for the present analysis. Then, the reception of the six signals was performed using the Arduino IDE software since the hardware contains a board of this same brand. In this stage is the signal that comes directly from the electrodes. This stage must ensure that this signal is not altered or lose the information of interest. To see the code used, see Annex 4. According to the same, the serial communication speed was 9600 baud, and the Delay, which is defined by the sampling time in ms, was 1, which means that the sampling occurs every ms. In addition, each analogue pin of the Arduino (A0 to A5) was defined as an input variable. In other words, each one being the input of one of the electrodes.

4.3.2. Processing the Signal with MATLAB

It was done in two phases using the MATLAB program (Figure 20). To see the code used, see Annex 5.

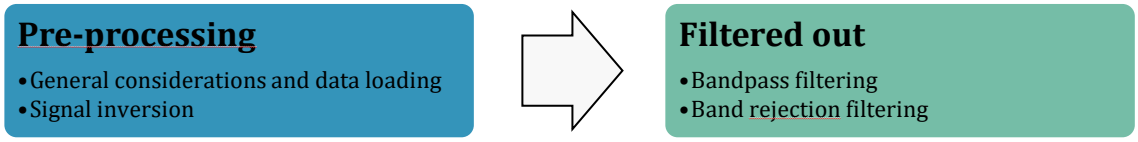

Figure 20. Measurements and processing of signal at MATLAB.

The first part, which is the pre-processing, was divided into two sections: 1) In the general considerations, a time of 5000 was assumed, a sampling duration of 10 seconds, and a sampling frequency of 500, i.e., every second 5000 samples are taken, because it is shown for 10 seconds the number of samples was 5000. The data obtained from Arduino IDE was integrated into MATLAB through a CSV file containing 5000 samples of each channel in each of its columns.

2) For the signal analysis in this phase follows the process of Pérez, 2016 [65]. First, an inversion of the signal was performed using the following formula. Where V_i and V_i^{INV} are vectors of 5000x1, where i= 1,...6, representing each channel. Subsequently, the $median_i$ (scalar) of each channel is calculated. In addition, the Arduino has input voltages between 0 and 5 volts and integrates them between the values 0 and 1023, which means a resolution of 5 V / 1024 units. Therefore, it is multiplied by a factor of 5/1024. Finally, the signal is amplified by multiplying by a factor of 60 to reach the heart rate values between 0.05 and 100 HZ, as shown in Table 1. Finally, as a result, is a vector of 500x1 that contains the amplified and inverted signal.

$$V_i^{INV} = (median_i - V_i) \times \frac{5}{1024} \times 60$$

For the second part, which is the filtering out, also it was divided into two sections: 1) bandpass filtering, which allows limiting the measurements to the frequency values cardiac that is between o.o5 and 100 Hz (see table 1). In addition, this reduces the EMG (electromyographic) signals that may have been captured; these are between 50 and 150 Hz. For filter considerations, it is of order 4. For the high-pass filter, the 'butter' function is used by both the filter is of the Butterworth type. The function must be passed the value of the filter order, the cutoff frequency between 0.05 - 100, and the type of filter (bandpass). To define the cutoff frequency, the sampling frequency (fs) is needed, and the parameter that passes is the cutoff frequency divided by half the sampling frequency and thus obtain a value between 0.05 and 100. The function returns two parameters that are the numerator (d) and denominator (c) of the transfer function of

the designed filter that will later be applied to implement the filter. Then, the 'filtfilt' function is applied where the filter is implemented.

2) Then, it was passed through a band rejection filter, which allows eliminating the frequencies produced by the electrical network in Ecuador is 60 HZ. The 'irrnotch' function was used; it also returns two values corresponding to the transfer function's numerator (b) and denominator (a). The central frequency (Wo) and bandwidth (BW) parameters must be passed to this function. The Wo is calculated the same as in the bandpass filter. The BW is the central frequency divided by the filter's quality coefficient.

Table 10. Explanation of codes used in MATLAB for filter design.

	Code	Explanation
Bandpass filter	`n=4`	filter order
	`fcutlow=0.05`	low cut frequency in Hz
	`fcuthigh=100`	high cut frequency in Hz
	`[d, c]= butter (n, [fcutlow,fcuthigh]/(fs/2),'bandpass')`	Use of 'butter' function to obtain the numerator and denominator
	`F1V1=filtfilt (d, c, V1inv)`	Use of 'filtfilt' function to apply the filter
Band rejection filter	`fcn=60;`	Filter cutoff frequency in Hz
	`Wo=fcn/(fs/2);`	Parameter for center frequency
	`BW=Wo/10;`	Filter bandwidth
	`[b, a] =iirnotch (Wo,BW);`	Use of 'iirnotch' function to obtain the numerator and denominator
	`F2V1= (filtfilt(b, a,F1V1))`	Use of 'filtfilt' function to apply the filter

4.4. Prediction

Once the best machine learning models are implemented, trained, and validated with datasets, it is time to confront them with new data. The Patient01 and Patient02 records and sECG images are new data. Next, identify the pathology of the untrained data, which has never been seen before. Here we use Python's *predict()* function, which allows you to predict the label of a new value based on the trained model. This function accepts only one parameter, which is the data to be tested. Therefore, it returns the label of the data passed as a parameter based on the learning or training data obtained from the model. In other words, the function acts on the trained model and uses the learned labels to assign and predict new data labels.

Chapter 5:

Results

5.1. Database Obtained

The first database contains 11,718 records, which are classified into five classes. The data set comprises 6-lead clinical ECG recordings of 10 seconds duration taken every 2 ms; that is, there were 5000 samples. To see an example of the data, see Table 14, where the graph of the 6 ECG channels and the numerical values that originate these graphs are shown.

Table 11. Example of ECG signals of Pyshionet at MATLAB for each of the classes.

	Graph the ECG channels for 10 seconds.	**Values in mV of the ECG channels during 10 microseconds.**
Norm - *Patient 5803*	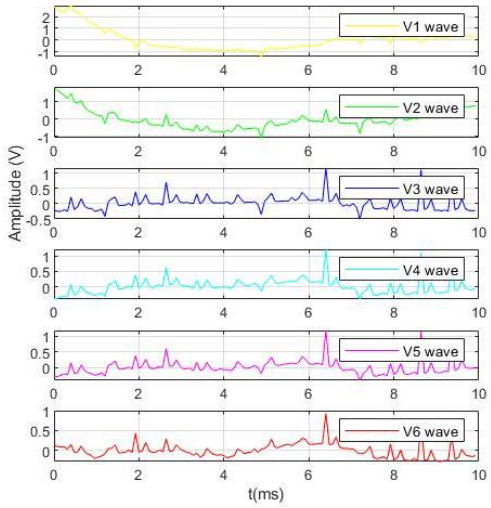	
CD - *Patient 2044*	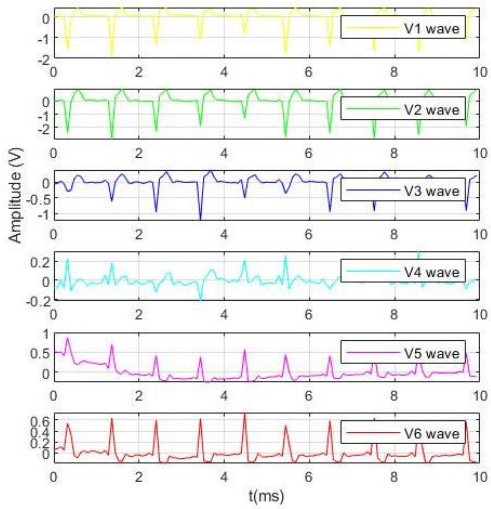	

Norm - *Patient 5803*

v1	**v2**	**v3**	**v4**	**v5**	**v6**
2.835	1.835	-0.23	-0.39	-0.285	0.14
2.615	1.64	-0.255	-0.38	-0.29	0.1
2.435	1.485	-0.265	-0.34	-0.245	0.09
2.285	1.335	-0.205	-0.3	-0.205	0.09
2.71	1.175	-0.26	-0.315	-0.235	0.04
2.925	1.46	0.205	0.075	0.15	0.15
2.475	0.975	-0.2	-0.285	-0.2	-0.05
2.315	0.92	-0.105	-0.2	-0.155	-0.035
2.23	1.055	0.155	0.03	0.085	0.115
1.875	0.66	-0.09	-0.145	-0.095	-0.03

CD - *Patient 2044*

v1	**v2**	**v3**	**v4**	**v5**	**v6**
0.025	0	-0.05	-0.08	0.525	0.07
0.02	-0.005	-0.045	-0.08	0.49	0.075
0.055	0.095	0.035	0.005	0.505	0.115
0.005	-0.015	-0.055	-0.08	0.405	0.05
-1.585	-2.39	-0.295	0.23	0.87	0.535
-0.16	-0.15	-0.255	-0.11	0.51	0.34
0.315	0.545	0.12	-0.04	0.22	-0.06
0.425	0.86	0.225	0	0.185	-0.085
0.21	0.56	0.165	0.015	0.255	0.02
0.05	0.065	-0.015	-0.02	0.28	0.035

HYP - *Patient 25*

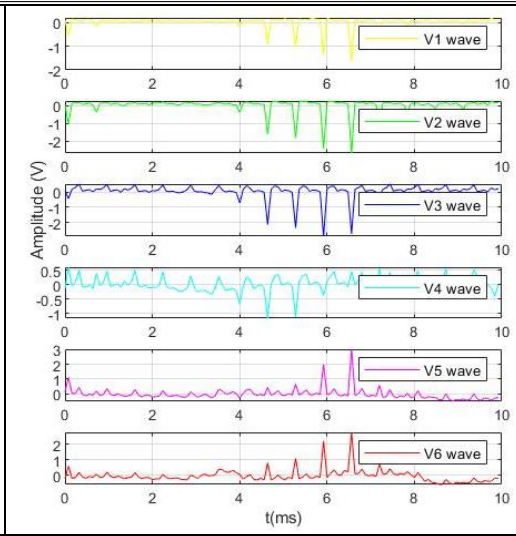

v1	v2	v3	v4	v5	v6
0.11	0.05	0.04	-0.145	0.145	-0.165
-0.53	-1.02	-0.425	0.605	1.11	0.6
0.145	0.16	0.185	-0.05	0.015	-0.19
0.12	0.17	0.305	0.095	0.035	-0.125
0.075	0.205	0.515	0.485	0.43	0.195
0.085	0.08	0.05	-0.065	-0.055	-0.1
0.115	0.13	0.115	-0.075	-0.135	-0.185
0.145	0.17	0.15	-0.01	-0.025	-0.07
0.07	0.03	0.015	-0.135	-0.09	-0.125
-0.165	-0.36	0.205	0.39	0.19	0.08

MI - *Patient 1124*

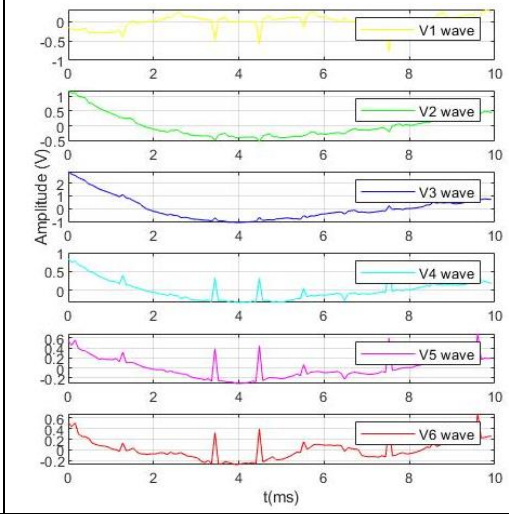

v1	v2	v3	v4	v5	v6
-0.15	1.19	2.885	0.835	0.55	0.52
-0.19	1.095	2.69	0.745	0.455	0.44
-0.22	1.12	2.585	0.775	0.56	0.51
-0.2	1	2.415	0.68	0.39	0.3
-0.2	0.97	2.305	0.635	0.355	0.255
-0.165	0.945	2.18	0.595	0.34	0.245
-0.3	0.785	1.915	0.505	0.3	0.22
-0.28	0.74	1.835	0.485	0.26	0.13
-0.285	0.66	1.695	0.435	0.225	0.105
-0.3	0.595	1.545	0.37	0.175	0.085

STTC - *Patient 9765*

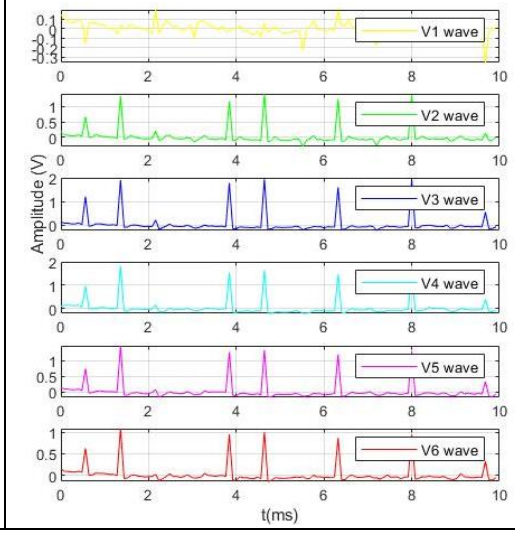

v1	v2	v3	v4	v5	v6
0.145	0.19	0.125	0.11	0.15	0.155
0.1	0.085	0.085	0.15	0.1	0.09
0.09	0.075	0.085	0.15	0.1	0.09
0.055	0.05	0.055	0.14	0.075	0.08
0.07	0.06	0.05	0.135	0.08	0.075
0.09	0.085	0.095	0.155	0.095	0.095
0.065	0.04	0.02	0.075	0.055	0.07
-0.16	0.67	1.205	0.975	0.75	0.63
0.06	-0.005	-0.05	0.005	-0.035	0
0.06	0.015	-0.02	-0.005	-0.005	0.01

The sECG images of Database 2 were constructed using the numerical values of database 1. To see an example of the sECG images, see table 12, which collects two random images for each class. The number of images produced was equal to the number of records mentioned in section 4.1, i.e., both databases contain the same number of parameters.

Table 12. Example of sECG images of Pyshionet at MATLAB for each of the classes.

Norm	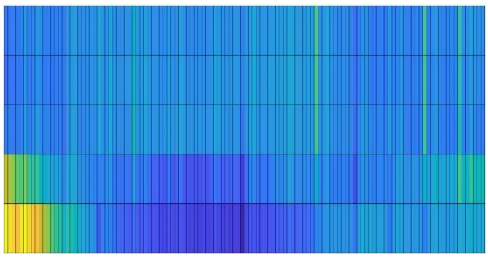 *Patient 5803*	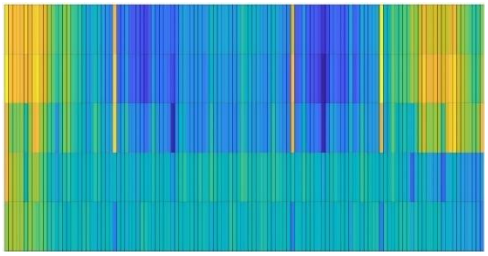 *Patient 6564*
CD	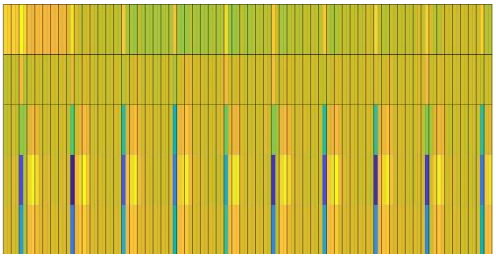 *Patient 2044*	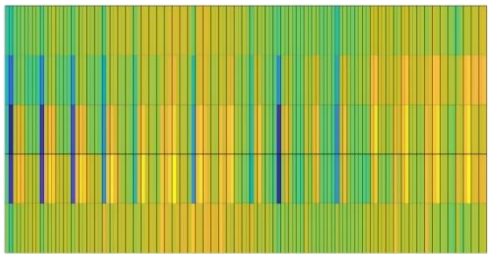 *Patient 942*
HYP	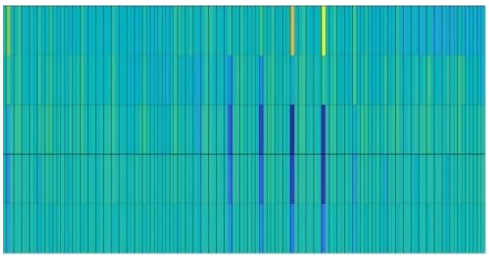 *Patient 25*	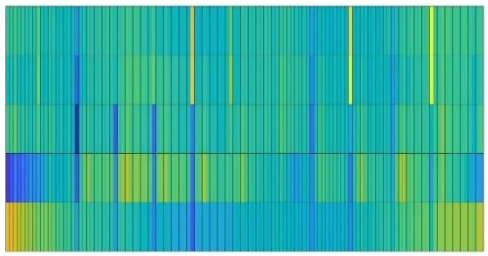 *Patient 105*
MI	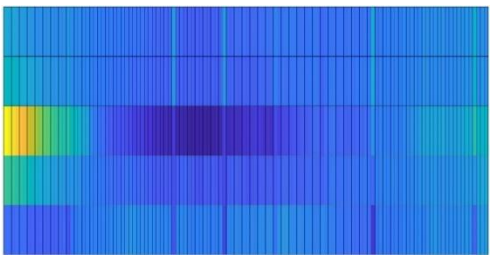 *Patient 1124*	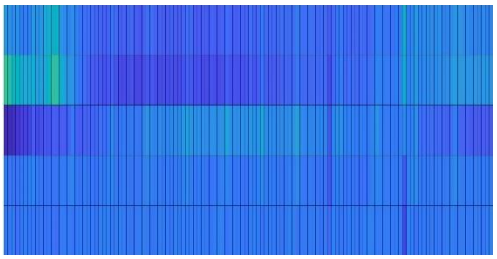 *Patient 1279*
STTC	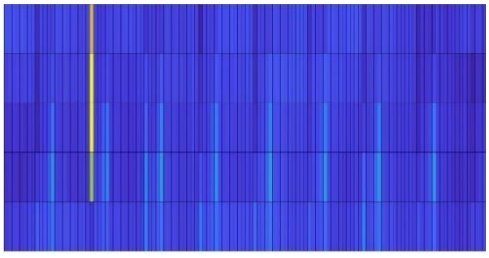 *Patient 9765*	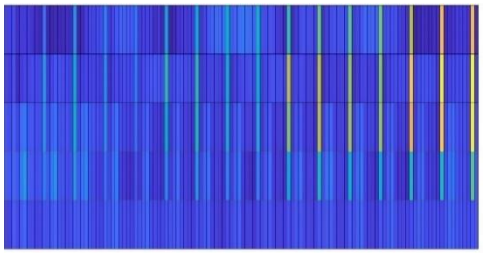 *Patient 494*

Each image contains one axis x = 125, i.e., from the 5000 samples of database 1 (samples every 0.002 sec), samples were taken every 0.080 sec. It is since the high amount of data did not allow to obtain visible plots. So, it was tested empirically until this value was reached. In addition, the y=6 axis corresponds to each of the channels of the leads. Finally, the Z-axis corresponds to the color provided by the amplitude of each of the signals.

5.2. Results of Neural Networks

5.2.1. Hyperparameters

To describe the model is essential, mentioning the hyperparameters used. This term refers to configuration variables external to the model itself and whose value [66]. In general, the data cannot be estimated, and the programmer adjusts the learning algorithms. First, the hyperparameters of two models related to the learning algorithm level: LSTM was trained of 12 epochs at approximately 4 hours, using a batch size of 500 and a learning rate of 1e-3. ResNet34 was trained of 48 epochs at approximately 2.5 hours, using a batch size of 14and a learning rate of 1e-3. Second, the hyperparameters related to structure and topology were the layers. The LSTM model comprises nine layers, excluding the input and output layers, and ResNet34 has 34 convolutional layers. Figure 18 and 19 shows the architecture of the neural networks.

The Activation layer is the most critical because it determines the output of one or more nodes through a function. For the first model, was used an output layer activation that is Sigmoid. The reason is that the NN fulfills the function of classification, and in turn, is a multiclass classification; that is, each input can be a single output value [67]. In other words, One node per class. The second model used a hidden layer activation function that was select according to the type of NN that is CNN [67]. Therefore, a ReLU activation function was used.

Then an Adam type optimizer is used in both models. It uses the first and second-moment estimates of the gradient to dynamically adjust the learning rate of each parameter [68]. In other words, after correcting the deviation, each iteration of the learning rate has a specific range, which makes the parameters stable [68]. In addition, to select the loss function, both models are multiclass classification, and the cross-entropy function is selected. It will calculate the cross-entropy loss between the correct category and the predicted category [69]. Finally, each of the models has its way of separating the trainset and validation set. For LSTM, it was divided as 82% and 18%, and for ResNet34, it was 80% and 20%, respectively. Table 13 shows all parameters used on time.

Table 13. Hyperparameters used in the training of neural networks

Hyperparameters	LSTM	ResNet34
Epoch number	12	48
Time of training	~ 4 hours	~2.5 hours
Batch size	500	14
Learning rate	1e-3	1e-3
# Layers	9	48

Activation Function	SoftMax	ReLU
Optimizer	Adam	Adam
Loss function	Categorical Cross-Entropy	Categorical Cross-Entropy
# Training dataset	9535 (82%)	9331 (80%)
# Validation dataset	2183 (18%)	2387 (20%)

5.2.2. Plots of Learning

First, Figure 21 shows the training results of the two networks. It can be seen how the networks evolve in terms of accuracy during the training after each iteration. From these graphs, both networks are progressing to reach a high training accuracy (blue lines) increases linearly with the epochs until it reaches almost 100%. There is a high accuracy when classifying data not seen before. However, the first network reaches a better result with fewer iterations than the second network. On the other hand, the validation test classification is the network's classification based on the previously learned features. This evaluation (orange lines) does not present the same uniformity. The first network has a maximum of 68%, while the second network exceeds 90%.

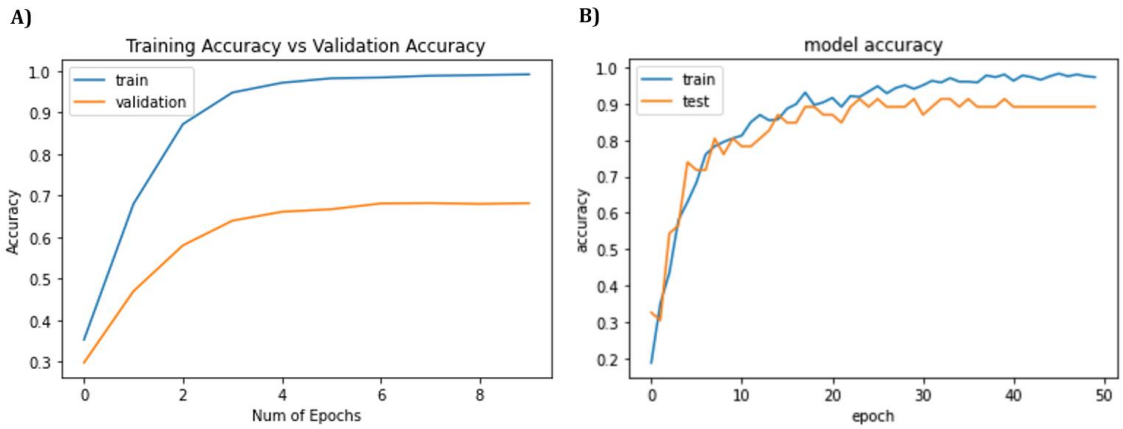

Figure 21. Plots of training and validation accuracy of the networks: A) LSTM NN and B) ResNet34.

On the other hand, as shown in Table 13, both models use the categorical cross-entropy function for the error calculation. This function allows comparing the actual distribution with the distribution predicted by the network, which is defined as:

$$L(y, y') = \sum_{j=0}^{M} \sum_{i=0}^{N} (y_{ij} \times \log(y'_{ij}))$$

The lower the value of this function, the more similar both distributions are, and the better is the model [70]. Figure 22 shows the evolution of the values of the Loss function during training. A. shows a characteristic behavior of a model with overfitting. Here the validation data reaches its

minimum after a few epochs and then starts to rise. In contrast, the Loss of the training data decreases linearly until it reaches almost 0, where it is maintained. B. the training loss decays after a few iterations, while the validation loss remains almost constant. Both decays resulted in relatively low errors, which shows the efficiency of the model.

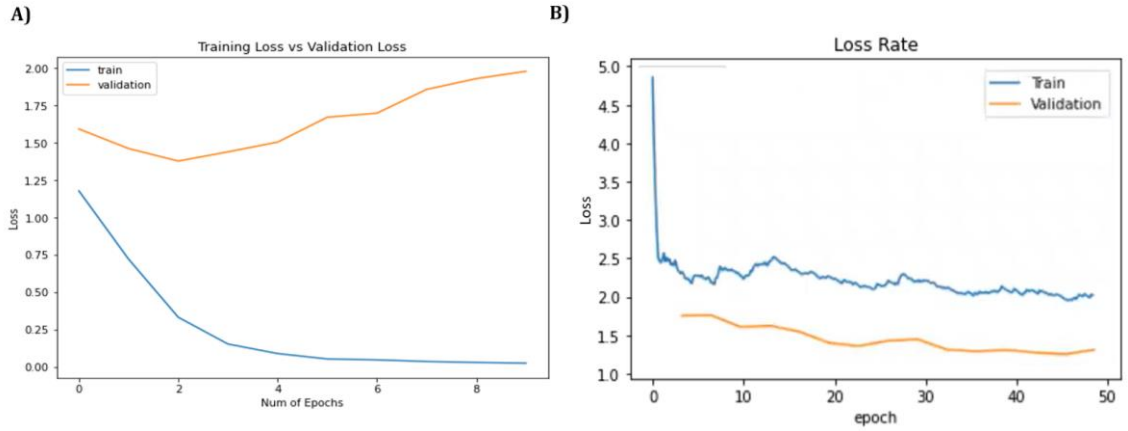

Figure 22. Plots of training and validation loss of the networks: A) LSTM NN and B) ResNet34

Both figures 21 and 22 are directly related since the higher the accuracy, the lower the value of the error in the network. In both graphs, both networks reach constancy, the first network in 6 iterations and the second in approximately 30 iterations. It can be interpreted as the networks start to overfit the training data. So, for future improvement, the amount of data could be increased.

5.2.3. Confusion Matrix

Then, the confusion matrix is used to evaluate the efficiency of the neural network. See Figure 23. The central diagonal data representation (drawn in blue) represents the number of hits in the model. Figure 23.A. shows the matrix confusion of LSTM NN, where a total of 2183 data were used in the validation dataset, of which 1493 were correctly classified, with an accuracy rate of 68.39%. The bottom of the main diagonal line shows false negatives or type II errors (the disease was not detected when it did exist); there are 253 such errors. Conversely, the upper of the main diagonal reflects the classifier error: false positive or error type I (disease detected but not present); there are 437such errors. On the other hand, figure 23.B. corresponds to the ResNet34 NN, where a total of 2387 data were used in the validation dataset, of which 2078 were correctly classified, with an accuracy rate of 73.81%. Also, there are 162 types II errors, and there are 147 error type I.

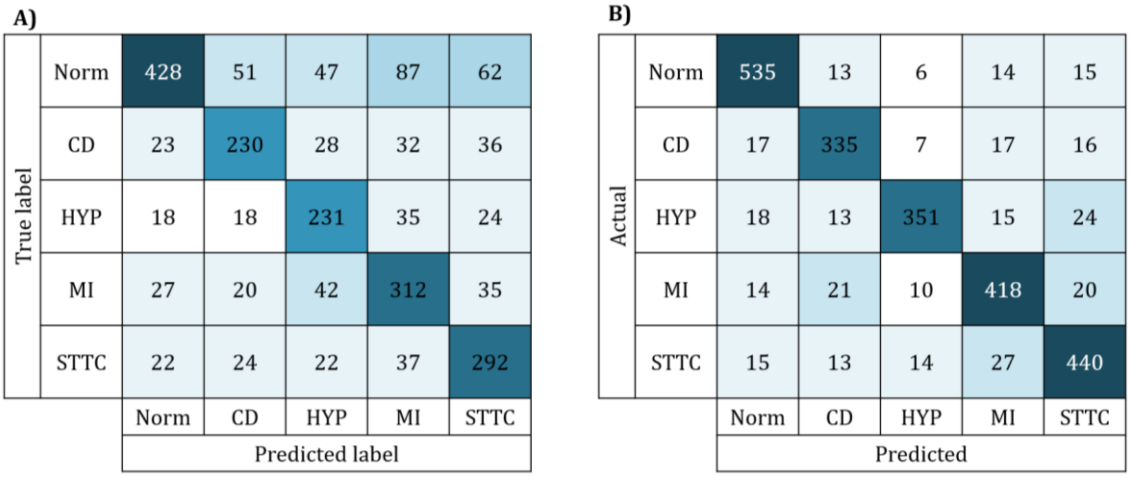

Figure 23. Confusion matrix: A) LSTM model and B) ResNet34 model.

5.2.4. Evaluation Metrics

Standard evaluation metrics, including sensitivity, recall, and accuracy, were implemented to perform a comprehensive performance evaluation. These metrics were calculated for each of the classes from the following formulas.

$$Recall = \frac{T_P}{T_P + F_N} \qquad Sensitivity = \frac{T_N}{T_N + F_P} \qquad Accurancy = \frac{T_P + T_N}{T_N + F_P + T_P + F_N}$$

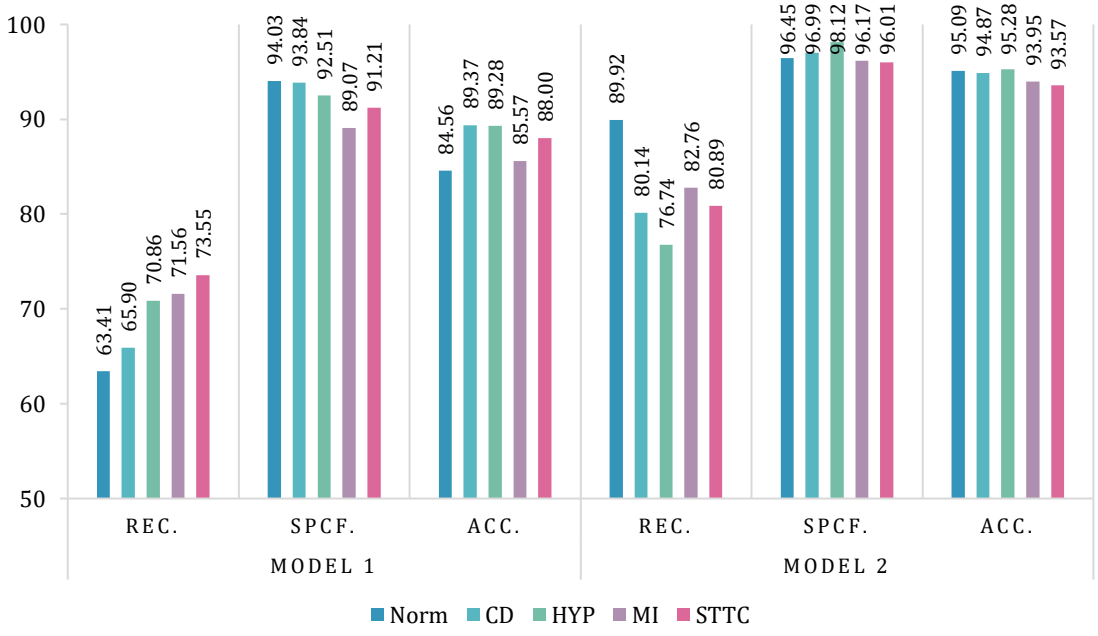

Figure 24. Recall, Specificity and Accuracy of 2 models of each class.

Figure 24 shows the metrics for each of the classes in each model. These metrics were calculated with the confusion matrices in Figure 23. The Recall values focus on type II errors (FN). A type II error occurs when a false null hypothesis is accepted. That is when the

prediction says that the disease has not been detected when it does exist. For both models, recall is > 62. Specificity values focus on type I errors (TF). A type I error occurs when a false null hypothesis is accepted. That is when the prediction says that a disease has been detected but is not present. For both models, the specificity is > 88. Finally, accuracy indicates how close the result of a measurement is to the actual value. For both models, the sparsity is> 84. All three metrics have values >50, indicating that the classes are balanced and a good model fit. On the other hand, model 2 has higher values in each of the metrics and each class.

5.3. Results of Exploratory Study

The signal results obtained according to section 4.3. for both patients are shown below.

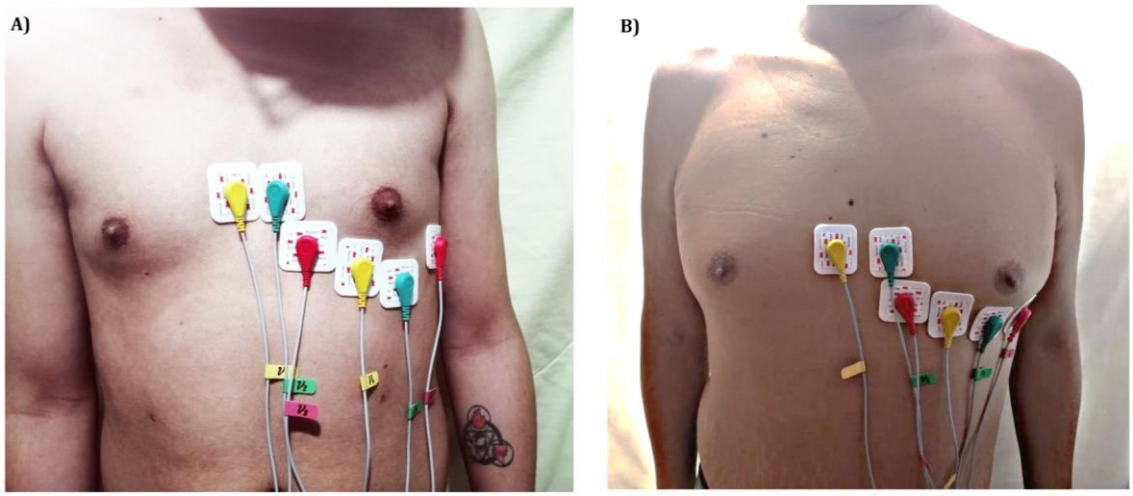

Figure 25. Patients during the measurement with the electrocardiograph: A) Patient01 and B) Patient02

The numerical data obtained in each of the steps produce the images in this section. As a result, Figures 26 and 27 show the six precordial leads processed and ready to be used in the NN. To see this process in more detail, see annexes 6 and 7. The signals corresponding to the patient01 that maintains the Norm condition contain much higher values. While the signals from patient02 that maintains the MI condition show relatively low values and little change. It may be since people who have had an episode of MI usually present unstable angina, ventricular arrhythmias, or heart block [56], [71]. Their heart function is usually at a lower-than-normal rate, and they often need help from external devices.

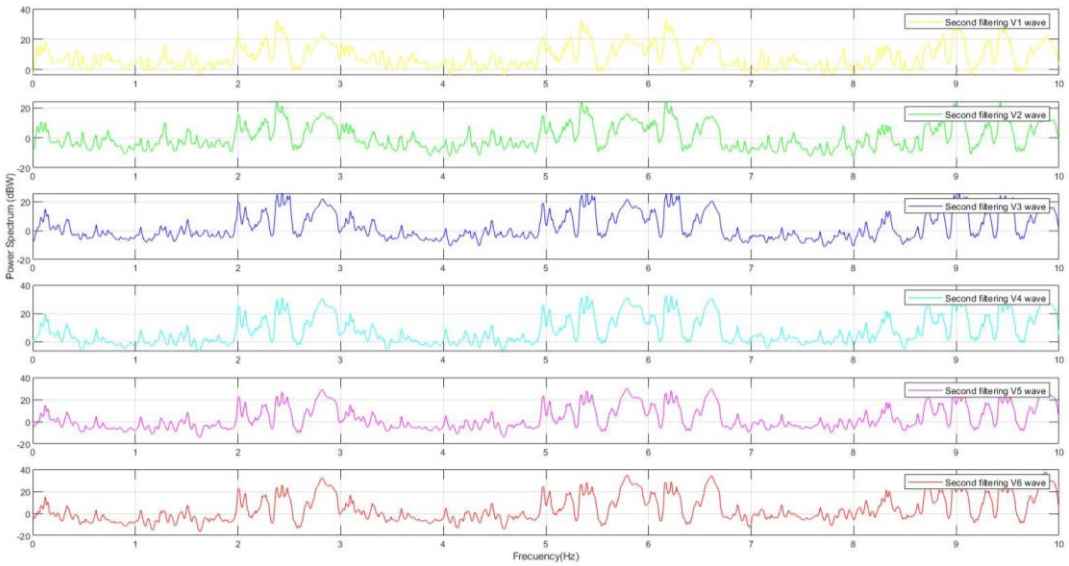

Figure 26. Plot at MATLAB of Patient01's ECG Precordial Waves applying a band-pass filter with a reject band of 60 Hz. Final signal.

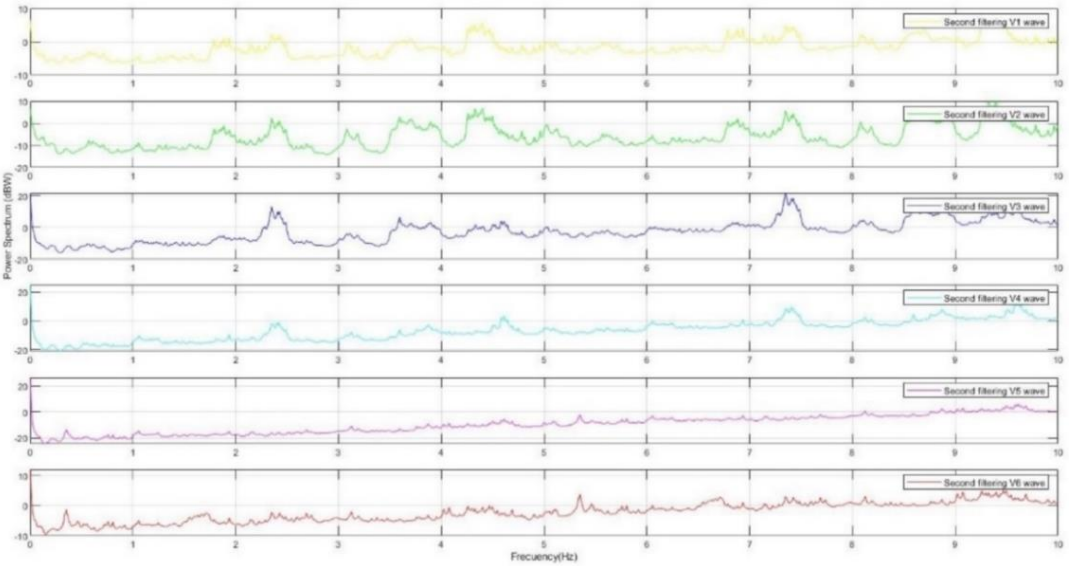

Figure 27. Plot at MATLAB of Patient02's ECG Precordial Waves applying a band-pass filter with a reject band of 60 Hz. Final signal.

Next, the processed Patient01 and Patient02 data went through the same process to obtain the sECG image corresponding to each one. In addition to this, to spatially understand the formation of the sECG images, look at figures 28 and 29. These represent three types of three-dimensional plots offered by MATLAB [72]. Figure A is a mesh surface used to give effect to a two-dimensional x×y matrix. Figure B is a surface plot that creates a colored three-dimensional surface instead of a mesh. Figure B from the top shows the sECG. Over time, the composition of the six channels provides a three-dimensional image that is also an sEMG distinguished by its colors. Figure C is a contour plot that represents two-dimensional, three-dimensional surfaces. Finally, Figure D combines the contour plot with a surface.

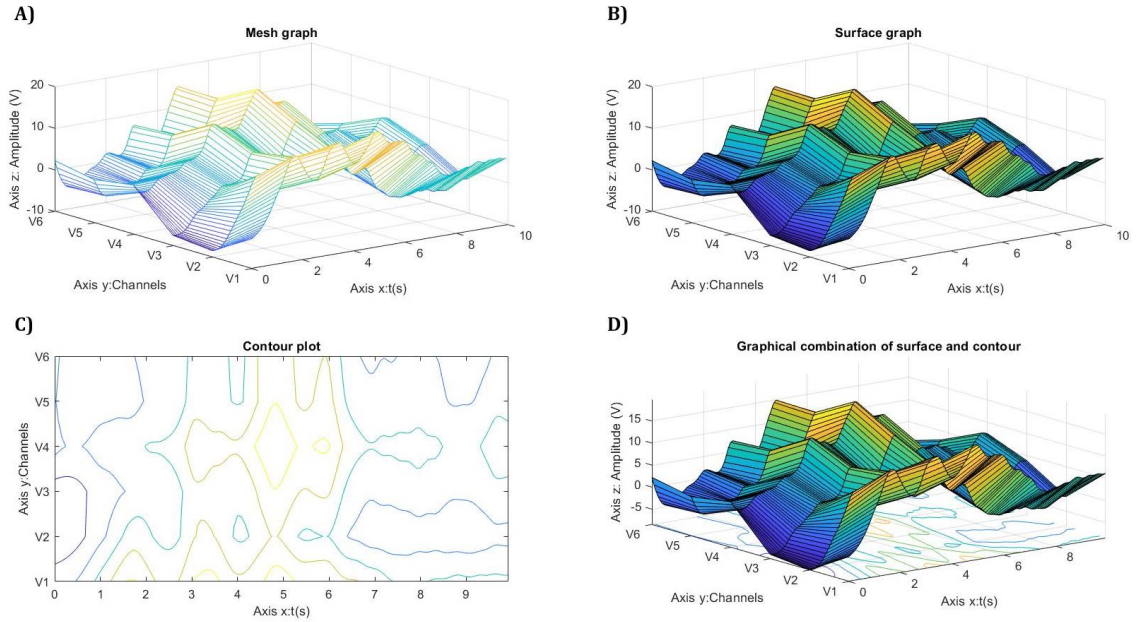

Figure 28. Three-dimensional plots at MATLAB: mesh surface plot, surface plot, and contour plot corresponding to Patient01.

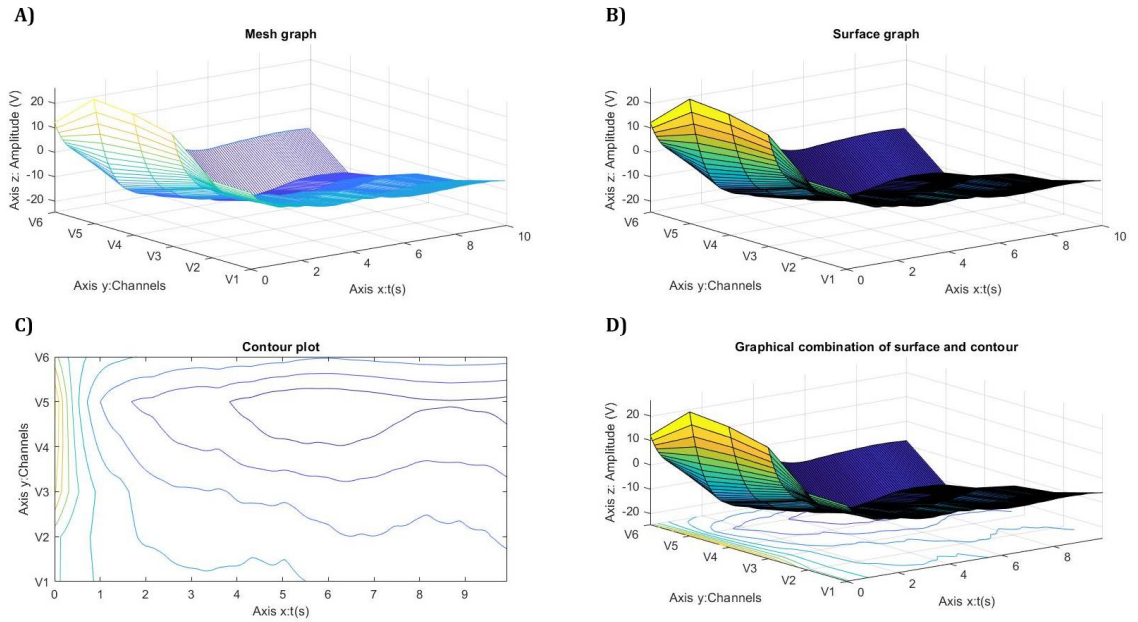

Figure 29. Three-dimensional plots at MATLAB: mesh surface plot, surface plot, and contour plot corresponding to Patient02.

Images 30 and 31 are the sECG images resulting from the exploratory study. Image 29, which corresponds to Patient01 with the normal condition, presents similarities with the images in Table 12. It shows sections where the colours are very light (voltage increase) and sections where dark colours are observed (voltage decrease). This image indicates the normal condition due to the nature of the cardiac cycle, which shows three positive waves and three negative waves. Image 31, which corresponds to Patient02 presenting the MI condition, also presents

similarities with the images in Table 12. Since this condition causes a drop-in heart rate and T-wave inversion, these images show a large percentage of dark colours. The few light-colored portions may be due to S-T segment elevation. Finally, in the STTC category, dark colours are also dominant, and some columns remain light colours, which may be due to S-T segment altitude.

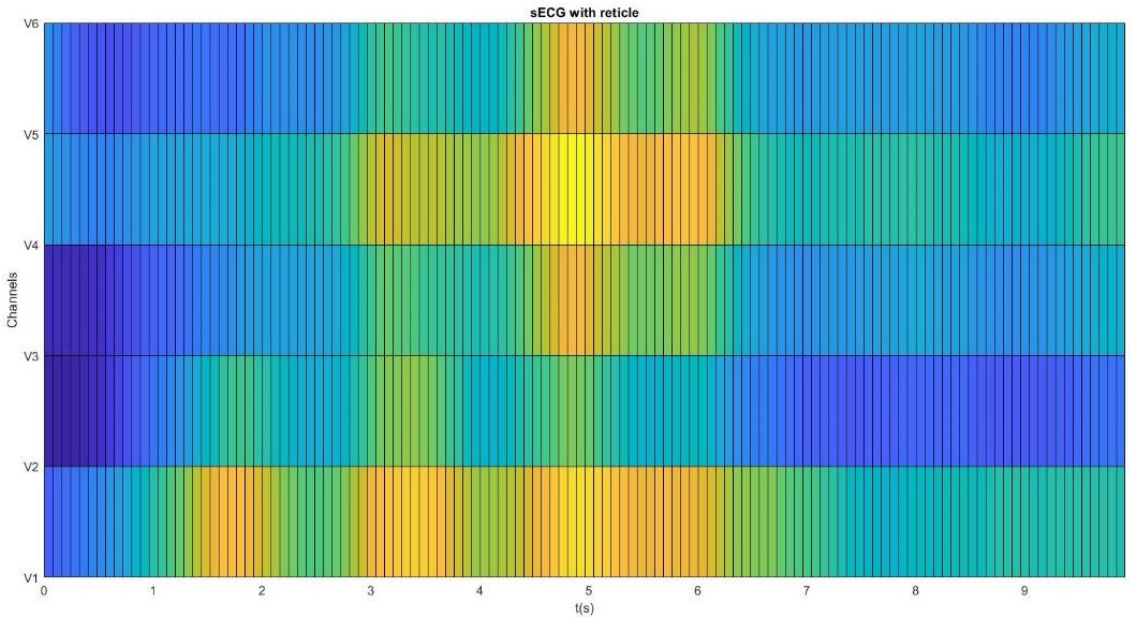

Figure 30. sECG image at MATLAB of the Patient01 after the preprocessing.

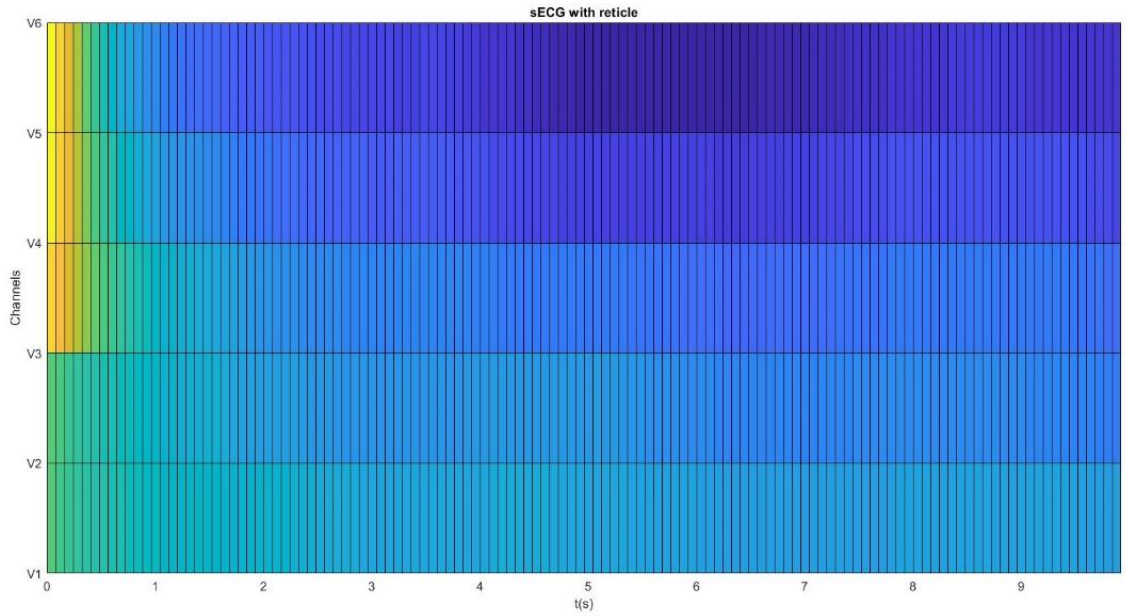

Figure 31. sECG image at MATLAB of the Patient02 after the preprocessing.

5.4. Prediction of Exploratory Study

The records and sECG images of patient01 and patient02 were run through the model. Both used the *model.predict()* function. Table 14 shows the results. On the one hand, the first patient in apparently normal condition, both networks concluded that he is class 0, which is equivalent to class Norm. On the other hand, the second patient who presented cardiac problems and an MI in the last two months received different predictions. Network 1 says that he is class 4, indicating STTC, which could be possible since these conditions can produce deficits in the distribution of blood in the heart. It is one of the possible future events of a person who has suffered an episode of MI. On the other hand, network 2 predicts that patient 02 is class 3, which corresponds to MI. this is another possible scenario. In both cases, the prediction of patient02 is possible.

Table 14. Results of patient prediction in both models.

	Red 1: LSTM NN	**Red 2: ResNet34 NN**
Patient01	`Category tensor (0)`	`Category tensor (0)`
Patient02	`Category tensor (4)`	`Category tensor (3)`

Chapter 6:

Discussion

6.1. Analysis of ECG Signals and sECG images

According to the analysis of ECG signals, which is the traditional way of performing an electrocardiogram, it has advantages such as the high sampling rate and the innumerable existing studies. However, the most used files for their storage: SCP-ECG, Digital Imaging, and Communication in Medicine Waveform Supplement 30 (DICOM-WS 30) and Health Level Seven Annotated Electrocardiogram (HL7 aECG) are complex to handle, which makes their processing difficult.

On the other hand, the sECG imaging proposed in this study is a new technique. It allows representing signal patterns that are difficult to identify in traditional signals, which is quite difficult considering that there are more than 20 types of pathologies. At the same time, sECG can be used to develop computer vision, which is the latest technology in artificial intelligence and therefore has great technological potential for the future. However, among its disadvantages are many channels required for its construction and the lack of studies of this type of sECG images, making a comparison with previous studies impossible. See Table 15 for more information.

Table 15. Advantages and disadvantages of ECG signals and sECG images.

	ECG signals (1D)	sECG images (2D)	Both
Advantages	▪ High sampling rate. ▪ Many studies with these signals.	▪ Visible amplitude patterns are difficult to see with the naked eye. ▪ This type of imaging can be used for computer vision.	▪ Having the ECG signals digitized. ▪ They are a safe, easy, and non-invasive method of recording the ECG signal. ▪ Allows visualization of the ECG signal over time.
Disadvantages	▪ The files in which they are stored are difficult to use.	▪ Requires a considerable number of channels for its construction. ▪ Null number of studies of this type of sECG images.	▪ "Cross talk" when there is crosstalk between ECG and EMG signals. ▪ Requires little storage space.

According to Table 12, the sECG images of the normal class present sections where the colors are very light (yellow) due to the increase in voltage. At the same time, there are sections where dark colors (blue) are observed, showing that the voltage is decreasing. In the CD class, the

dominant colors are yellow, which may be since the heart rate is elevated in this condition. It also presents certain columns with dark colors, which may be due to the variations suffered by the signal in the R-R interval characteristic of this condition. In the HYP class, the dominant color is bluish-green, which may be due to negative T waves, negative P waves in lead V1 and depressions of S waves in leads V1 and V2. At the same time, the clear sections may be due to high R waves and S-T segment elevation. In the MI class, dark colors dominate since this condition produces a decrease in heart rate and T-wave inversion. While the few sections with light colours may be caused by S-T segment elevation. Finally, the STTC class is also dominated by dark colours and with several columns maintaining light colours, which may be due to S-T segment elevations.

6.2. Analysis of NN and Exploratory Study

This research described how to use RNNs (LSTM) and CNNs (ResNet34) to detect cardiac pathologies. First, the role of LSTMs is to classify number sequences. In other words, it transforms the data entered so that it circulates through the network even in the following instant of time. On the other hand, the function of ResNet34 can be defined as extract high-level visual features over time. It extracts these visual characteristics from the mesh on the Z-axis projected in time and the channels, X and Y axes.

Model 1 (LSTM) works with cardiac signals (1D) and model 2 (ResNet34) works with sECG images (3D). Both models were designed to classify ECG signals into five classes: Norm, CD, HYP, MI, and STTC. For which their databases used 11,718 records of ECG signals of 6 precordial leads. According to the tests performed in section 5.2., it can be affirmed that the LSTM is more economical since it can be trained with a normal CPU and RAM according to the hyperparameters sectioned. The ResNet34 needs a GPU and High RAM; it so demands more computational resources. On the other hand, the training time of the LSTM (4 hours) is longer than that of the ResNet34 (2.5 hours).

According to the learning rate in the training set, LSTM reaches a higher value (98.71%) than ResNet34 (93.65%). However, the learning rate of the validation set, the LSTM, is surpassed by 68.39% by the ResNet34 (87.05%). See Figure 21. Here it is important to highlight that the validation set is where the efficiency of the network is tested, so the ResNet has better results. In turn, this learning rate of the validation set is reflected in the confusion matrices (Figure 23), where the LSTM has 230 types ii errors and 437 type I errors. While the ResNet has 162 types II errors, and there are 147 type I errors. Finally, in the metrics analysis, the values obtained in recall and specificity are higher for the ResNet, while the accuracy is

higher for the LSTM. It can be said that LSTM has better learning while training, while ResNet is better at making accurate predictions. Looking at all these characteristics in Table 16 confirms that ResNet performed better.

Table 16. Summarize of evaluation of two models.

Method	Environment used	Time of training	Type of data	Metrics (%)			Errors	
				Train set	Validation set		Type I	Type II
				Acc.	Rec.	Spcf.		
LSTM NN	CPU	~4 hours	Numeric ECG signal	98.71	89.06	92.13	437	230
ResNet34	GPU	~2.5 hours	sECG Images	93.65	89.64	93.42	147	162

6.3. Comparison with Other Studies

This study uses two learning models; the difference is the type of input used. So, this comparison is based on several aspects such as input, application, and the number of channels used. See Table 17.

Table 17. Different methods of using numerical and images data present in the literature.

	Method	Application	# Parameters	Metrics (%)			Ref.
				Rec.	Spcf.	Acc.	
Numerical data	LSTM NN Present work	Classification of Norm, CD, HYP, MI, and STTC	11,718 records of 6 precordial leads	89.06	92.13	98.71	-
	Deep residual CNN	ECG Heartbeat Classification	290 records of lead II	95.10	-	95.90	[54]
	LSTM and algorithms	Continuous cardiac monitoring	~50000 records of single channel ECG	99.20	93.00	99.20	[55]
	LSTM and algorithms	Classification MI and Norm condition	12359 records of 15 leads	98.49	97.97	-	[58]
	FIS (ANN) and algorithms	Classification MI and Norm condition	200 records of single channel ECG signal	73.00	-	-	[56]
	N-Net	Detection of MI	240 records of 12 leads	-	-	95.76	[57]
	MSN-Net	Detection of MI	240 records of 12 leads	-	-	61.82	[57]
Images data	ResNet34 Present work	Classification of Norm, CD, HYP, MI, and STTC	11,718 sECG images of 6 precordial leads	89.64	93.42	93.65	-
	KNN	Detection EMG signal of finger movements	240 images sEMG of 24 channels	-	95.70	97.70	[59]
	HD	Detection EMG signal of finger movements	30 images sEMG of 64 channels	-	-	96.64	[60]
	Deep CNN	Gesture recognition	79 images sEMG of 129 channels	-	96.70	65.10	[16]

	SQI with dense CNN	Classifier AF from normal sinus rhythm, other rhythms, and noise	8,528 spectrograms of single channel ECG signal	-	-	80.00	[73]

** Rec: Recall, Spcf: Specificity, Acc: Accuracy, ML: Machine Learning, CNN: Convolutional Neural Network, ANN: Artificial Neural Networks, FIS: Fuzzy Inference System, N-Net: multi-lead features-concatenate narrow network, MSN-Net: multi-scale features-concatenate networks, KNN: K Nearest Neighbor (supervised ML algorithm), HD: High-dimensional computing (supervised ML algorithm), SQI: Signal Quality Index, AF: Atrial fibrillation.

For the first model, the LSTM NN obtained a recall of 89.06%, a Specificity of 92.13%, and an Accuracy of 98.71%. All three metrics are pretty good and comparable with other similar models. It was compared with other classifiers for cardiac conditions such as CNN, FIS, N-Net, MSN-Net, and LSTM. All of them are usually used as classifiers. Although the values of the metrics are similar to those of existing studies, it is important to highlight three features:

- The amount of data in the numerical data is relatively high when standardizing and collecting from several databases or quite low when using a single database.
- Although most of them have an application of classification or detection of pathologies, there is no variety in classes since they are limited to only 2.
- The channels analyzed are 1 or 12, which are those performed with devices at the clinical level; there is no variety in the analysis by channels.

For the second model, the ResNet34 NN obtained a recall of 89.64%, a Specificity of 93.42%, and an Accuracy of 93.65%. The same values are at the same level as other models that use sECG images as inputs. The methods with which compare include KNN, HD, CNN, and SQI. While the values of the metrics are similar to existing studies, it is important to highlight three features such as:

- There are studies in sEMG images, not with sECG images.
- There is a study of electrocardiographic signals with spectrogram images, but it comes back to the issue of channels since there is only one channel.
- There is no database for surface images (sECG, sEMG, sECG, and others), so the images that exist are of electromyography and a concise quantity.

Chapter 7:

Conclusions & Outlook

7.1. Conclusions

It can be concluded that there are many ECG signal databases, but they usually contain a short number of signals. Putting these databases together represents a challenge since standardizing them is complicated by the equipment, channels, and conditions such as frequency. The database used in this study is the only one that contains a significant amount of data, which allowed a better study.

It was also found that there are no studies that focus on precordial leads, even though they are fundamental for the detection of anomalies. Moreover, in the field of surface signals, it is an entirely new and unexplored field. Particularly for sECG images, no studies have been found that mention or study them. Biomedical signals are vast and proposing new ways to perform measurements helps the physician provide a more accurate diagnosis and treatment as soon as possible.

In addition, it can be affirmed that the two predictive models built have great efficiency, through the analysis of the metrics: specificity, sensitivity, and precision. The first, Long Short-Term Memory that uses as input the numerical values captured by clinical electrocardiographs, and the second, Residual Neural Network that uses sECG images as input. And most importantly, it showed that the use of sECG images equals and exceeds the conventional model used so far. Likewise, it showed better results with previous studies related to the subject.

In addition, it was found that the electrocardiograph is the essential device in detecting most cardiac pathologies. The design proposed in this study was effortless, an electrocardiograph for precordial measurements. These signals, being unipolar, were captured one at a time, i.e., the result is six individual signals. Although it consisted of simple hardware, its strength was based on the signals' amplification, preprocessing, and digital treatment. It reduces the economic gap presented to the patient when a study of this type is performed. The results obtained were signals quite similar to those taken clinically.

Finally, it was found that this DSS is being used more and more in recent years. The machine learning models are ideal for supporting the primary care physician, for being a software to

support the diagnosis, but not to replace the health professional. The proposed models are at the level of previously conducted studies, with certain advantages, such as the number of data, the number of channels, and the introduction of new inputs such as the sECG images.

7.2. Future Works

It is recommended to perform studies using several leads, not the usual three leads. Although the electrocardiograph was simple, better results can be obtained if the amplification and filtering stages are performed physically, i.e., with physical components. It is recommended to work on the construction of large, current databases with good metadata content. Although metadata was not used in this study, these indicators could provide more information to the physician to make a better diagnosis. It is recommended to work with machine learning models that allow the construction of a new DSS to evaluate cardiac pathologies better. Finally, it is recommended that the field of sECG be further explored since the results obtained in this study show that it can represent a significant improvement in how cardiac diagnosis is performed on an active basis.

References

[1] WHO, "¿Qué son las enfermedades cardiovasculares?" https://www.who.int/cardiovascular_diseases/about_cvd/es/ (accessed May 28, 2021).

[2] WHO, "Ecuador: WHO statistical profile," 2012. Accessed: Jul. 09, 2021. [Online]. Available: https://www.who.int/gho/countries/ecu.pdf?ua=1.

[3] INEC, "Anuario de Estadísticas Vitales - Nacimientos y Defunciones 2014," Quito, 2014. Accessed: Jul. 09, 2021. [Online]. Available: https://www.ecuadorencifras.gob.ec/documentos/web-inec/Poblacion_y_Demografia/Nacimientos_Defunciones/Publicaciones/Anuario_Nacimientos_y_Defunciones_2014.pdf.

[4] PAHO, "Factores de riesgo para las enfermedades crónicas no transmisibles en Ecuador," Mar. 2016. Accessed: Jul. 09, 2021. [Online]. Available: https://www.paho.org/ecu/index.php?option=com_content&view=article&id=1694-21-de-marzo-inicia-encuesta-step-sobre-factores-de-riesgo-para-las-enfermedades-cronicas-no-transmisibles-ecnt-en-el-recreo-del-canton-duran-con-la-utilizacion-de-dispositivos-moviles&catid=297&Itemid=360.

[5] MSP, "MSP previene enfermedades cardiovasculares," 2020. https://www.salud.gob.ec/msp-previene-enfermedades-cardiovasculares-con-estrategias-para-disminuir-los-factores-de-riesgo/ (accessed Jul. 09, 2021).

[6] Institute Texas Heart, "Heart Information Center: Heart Disease Risk Factors." https://www.texasheart.org/heart-health/heart-information-center/topics/heart-disease-risk-factors/ (accessed Jul. 09, 2021).

[7] C. Stanfield and W. Germann, "Principles of Human Physiology: International Edition," 3rd ed., Pearson.

[8] L. Williams and P. Wilkins, *ECG Interpretation Made Incredibly Easy!*, 5th editio. London: Wolters Kluwer, 2011.

[9] ECG & ECHO LEARNING, "Cardiac electrophysiology: action potential, automaticity and vectors," in *Clinical ECG Interpretation*, .

[10] Medical & Biological Sciences, "Why is the P wave smaller than the QRS complex? | Draw It to Know It." https://www.drawittoknowit.com/pop-quizzes/physiology/why-is-the-p-wave-smaller-than-the-qrs-complex (accessed Jul. 09, 2021).

[11] J. F. Guerrero Martínez, "Tema 2 Bioseñales," in *INGENIERÍA BIOMÉDICA* , 2010.

[12] R. Merletti and S. Muceli, "Tutorial. Surface EMG detection in space and time: Best practices," *J. Electromyogr. Kinesiol.*, vol. 49, no. October, p. 102363, 2019, doi: 10.1016/j.jelekin.2019.102363.

[13] R. Merletti, A. Botter, A. Troiano, E. Merlo, and M. Alessandro, "Technology and instrumentation for detection and conditioning of the surface electromyographic signal : State of the art," *Clin. Biomech.*, vol. 24, no. 2, pp. 122–134, 2009, doi: 10.1016/j.clinbiomech.2008.08.006.

[14] H. Urbanek and P. van der Smagt, "IEMG: Imaging electromyography," *J. Electromyogr. Kinesiol.*, vol. 27, pp. 1–9, Apr. 2016, doi: 10.1016/J.JELEKIN.2016.01.001.

[15] H. Shin, Y. Zheng, and X. Hu, "Variation of Finger Activation Patterns Post-stroke Through Non-invasive Nerve Stimulation," *Front. Neurol.*, vol. 9, no. December, pp. 1–7, 2018, doi: 10.3389/fneur.2018.01101.

[16] W. Geng, Y. Du, W. Jin, W. Wei, Y. Hu, and J. Li, "Gesture recognition by instantaneous surface EMG images," *Sci. Rep.*, vol. 6, no. June, pp. 6–13, 2016, doi: 10.1038/srep36571.

[17] L. Shaw and S. Bagha, "Online Emg Signal Analysis for Diagnosis of Neuromuscular Diseases By Using Pca and Pnn," *Int. J. Eng. Sci.*, vol. 4, no. 10, pp. 4453–4459, 2012.

[18] M. I. Ferrer, “The Development of the Electrocardiogram,” *Am. Surg.*, vol. 61, no. 6, pp. 39–46, 1984, doi: 10.1007/978-1-4613-3834-5_3.
[19] Pardell Xavier, “Sistemas de Instrumentación Médica - Apuntes de Electromedicina,” Aug. 06, 2021. https://www.pardell.es/instrumentacion-medica.html (accessed Sep. 22, 2021).
[20] “P12 Smart Bracelet Black Smart Wristband Sale, Price & Reviews | Gearbest.” https://www.gearbest.com/smart-wristband/pp_009360507991.html (accessed Jul. 09, 2021).
[21] “Qardio Core Wireless ECG Monitor.” https://www.coolthings.com/qardio-core-medical-grade-ecg-monitor/ (accessed Jul. 09, 2021).
[22] “Portable ECG Monitor with Color LCD Touchscreen.” http://www.globalcaremarket.com/es/portable-ecg-monitor-with-color-lcd-touchscreen.html (accessed Jul. 09, 2021).
[23] “Electrocardiograma (ECG): ¿Cuál es el mejor del 2021?” https://www.reviewbox.com.mx/electrocardiograma/ (accessed Jul. 09, 2021).
[24] “¿Qué es Arduino? ,” *Arduino.cl*. https://arduino.cl/que-es-arduino/ (accessed Aug. 25, 2021).
[25] Process Integral, “ARDEV034WO0036 B MANUAL DE INSTRUCCIONES CABLES ECG PARA PACIENTES,” Accessed: Aug. 25, 2021. [Online]. Available: www.integral-process.com.
[26] “3M™ Red Dot™ Electrodos de monitorización.” https://www.3m.com.es/3M/es_ES/p/d/v000057870/ (accessed Aug. 25, 2021).
[27] Oracle, “What Is a Database.” https://www.oracle.com/database/what-is-database/ (accessed Aug. 11, 2021).
[28] S.-C. Wang, “Artificial Neural Network,” *Interdiscip. Comput. Java Program.*, pp. 81–100, 2003, doi: 10.1007/978-1-4615-0377-4_5.
[29] S. Hochreiter and J. Schmidhuber, “Long Short-Term Memory,” *Neuronal Comput.*, vol. 9, no. 8, pp. 1735–1780, 1997, Accessed: Aug. 24, 2021. [Online]. Available: http://www.bioinf.jku.at/publications/older/2604.pdf.
[30] “Understanding LSTM Networks,” Aug. 27, 2015. https://colah.github.io/posts/2015-08-Understanding-LSTMs/ (accessed Aug. 24, 2021).
[31] P. Ruiz, “Understanding and visualizing ResNets,” *Towards Data Science*, Oct. 08, 2018. https://towardsdatascience.com/understanding-and-visualizing-resnets-442284831be8 (accessed Aug. 25, 2021).
[32] M. Gao, J. Chen, H. Mu, and D. Qi, “A transfer residual neural network based on resnet-34 for detection of wood knot defects,” *Forests*, vol. 12, no. 2, pp. 1–16, Feb. 2021, doi: 10.3390/F12020212.
[33] “Google Colab,” *Google Research*. https://research.google.com/colaboratory/intl/en-GB/faq.html (accessed Aug. 25, 2021).
[34] Python.org, “What is Python? Executive Summary.” https://www.python.org/doc/essays/blurb/ (accessed Aug. 25, 2021).
[35] MathWorks, “MATLAB - El lenguaje del cálculo técnico.” https://es.mathworks.com/products/matlab.html (accessed Aug. 25, 2021).
[36] “Software | Arduino.” https://www.arduino.cc/en/software (accessed Aug. 25, 2021).
[37] “Why TensorFlow.” https://www.tensorflow.org/about (accessed Aug. 25, 2021).
[38] “About Keras.” https://keras.io/about/ (accessed Aug. 25, 2021).
[39] fastai, “Welcome to fastai.” https://docs.fast.ai/ (accessed Aug. 25, 2021).
[40] C. K. Alexander and M. N. O. Sadiku, *Fundamentos de Circuitos Eléctricos 3th edition*. 2009.
[41] P. Wagner *et al.*, “PTB-XL, a large publicly available electrocardiography dataset,” *Sci. Data*, vol. 7, no. 1, Dec. 2020, doi: 10.1038/S41597-020-0495-6.
[42] J. Carreño, F. Apablaza, M. Ocaranza, and J. Jalil, “Cardiac Hypertrophy: Molecular and Cellular Events,” *Rev. Española Cardiol. (English Ed.*, vol. 59, no. 5, pp. 473–486, May 2006, doi: 10.1016/S1885-5857(06)60796-2.

[43] Cardioalianza, “Infarto de Miocardio ,” 2018. https://cardioalianza.org/las-enfermedades-cardiovasculares/infarto-de-miocardio/ (accessed Jul. 09, 2021).
[44] S. Lome, “Causes of T wave, ST Segment Abnormalities | LearntheHeart.com.” https://www.healio.com/cardiology/learn-the-heart/blogs/68-causes-of-t-wave-st-segment-abnormalities (accessed Aug. 24, 2021).
[45] Mayo Clinic, “Heart arrhythmiaMayo Clinic,” 2021. https://www.mayoclinic.org/diseases-conditions/heart-arrhythmia/diagnosis-treatment/drc-20350674 (accessed Jul. 09, 2021).
[46] “Left Ventricular Hypertrophy on the Electrocardiogram,” *My EKG, The Web of the Electrocardiogram*, 2013. https://en.my-ekg.com/hypertrophy-dilation/left-ventricular-hypertrophy.html (accessed Jul. 09, 2021).
[47] Y. F. Low, I. B. Mustaffa, N. B. M. Saad, and A. H. Bin Hamidon, “Development of PC-based ECG monitoring system,” *SCOReD 2006 - Proc. 2006 4th Student Conf. Res. Dev. "Towards Enhancing Res. Excell. Reg.*, pp. 66–69, 2006, doi: 10.1109/SCORED.2006.4339310.
[48] M. Ehnesh, P. Abatis, and F. S. Schlindwein, “A portable electrocardiogram for real-time monitoring of cardiac signals,” *SN Appl. Sci. 2020*, vol. 2, no. 8, pp. 1–11, Jul. 2020, doi: 10.1007/S42452-020-3065-9.
[49] M. Bansal and B. Gandhi, “IoT Big Data in Smart Healthcare (ECG Monitoring),” *Proc. Int. Conf. Mach. Learn. Big Data, Cloud Parallel Comput. Trends, Prespectives Prospect. Com. 2019*, pp. 390–396, Feb. 2019, doi: 10.1109/COMITCON.2019.8862197.
[50] H. Kim *et al.*, “A configurable and low-power mixed signal SoC for portable ECG monitoring applications,” *IEEE Trans. Biomed. Circuits Syst.*, vol. 8, no. 2, pp. 257–267, 2014, doi: 10.1109/TBCAS.2013.2260159.
[51] A. Martín-Yebra *et al.*, “Studying heart rate variability from ballistocardiography acquired by force platform: Comparison with conventional ECG,” *Comput. Cardiol. (2010).*, vol. 42, pp. 929–932, Feb. 2015, doi: 10.1109/CIC.2015.7411064.
[52] J. Granados, T. Westerlund, L. Zheng, and Z. Zou, “IoT platform for real-time multichannel ECG monitoring and classification with neural networks,” *CONFENIS 2017*, vol. 310, pp. 181–191, 2018, doi: 10.1007/978-3-319-94845-4_16.
[53] W. Alhalabi, “Patient monitoring at home using 32-channel cost-effective data acquisition device,” *Telemat. Informatics*, vol. 35, no. 4, pp. 883–891, Jul. 2018, doi: 10.1016/J.TELE.2017.12.004.
[54] M. Kachuee, S. Fazeli, and M. Sarrafzadeh, “ECG heartbeat classification: A deep transferable representation,” *Proc. - 2018 IEEE Int. Conf. Healthc. Informatics, ICHI 2018*, pp. 443–444, 2018, doi: 10.1109/ICHI.2018.00092.
[55] S. Saadatnejad, M. Oveisi, and M. Hashemi, “LSTM-Based ECG Classification for Continuous Monitoring on Personal Wearable Devices,” *IEEE J. Biomed. Heal. Informatics*, vol. 24, no. 2, pp. 515–523, 2020, doi: 10.1109/JBHI.2019.2911367.
[56] A. N. Ardan, M. Ma’arif, Z. H. Aisyah, M. Olivia, and S. M. Titin, “Myocardial infarction detection system from PTB diagnostic ECG database using Fuzzy inference system for S-T waves,” *J. Phys. Conf. Ser.*, vol. 1204, no. 1, pp. 1–7, 2019, doi: 10.1088/1742-6596/1204/1/012071.
[57] J. Z. Jian *et al.*, “Detection of myocardial infarction using ecg and multi-scale feature concatenate,” *Sensors*, vol. 21, no. 5, pp. 1–17, Mar. 2021, doi: 10.3390/S21051906.
[58] A. Darmawahyuni *et al.*, “Deep Learning with a Recurrent Network Structure in the Sequence Modeling of Imbalanced Data for,” *MDPI, Algotithms*, vol. 12, pp. 1–12, 2019, doi: 10.3390/a12060118.
[59] I. Topalović, S. Graovac, and D. B. Popović, “EMG map image processing for recognition of fingers movement,” *J. Electromyogr. Kinesiol.*, vol. 49, p. 102364, 2019, doi: 10.1016/j.jelekin.2019.102364.
[60] A. Moin *et al.*, “An EMG Gesture Recognition System with Flexible High-Density Sensors and Brain-Inspired High-Dimensional Classifier,” *Proc. - IEEE Int. Symp.*

Circuits Syst., vol. 2018-May, 2018, doi: 10.1109/ISCAS.2018.8351613.
[61] "PTB-XL, a large publicly available electrocardiography dataset v1.0.1." https://physionet.org/content/ptb-xl/1.0.1/ (accessed Aug. 11, 2021).
[62] G. J. Mandellos, M. N. Koukias, I. S. Styliadis, and D. K. Lymberopoulos, "E-SCP-ECG + protocol: An expansion on SCP-ECG protocol for health telemonitoringpilot implementation," *Int. J. Telemed. Appl.*, 2010, doi: 10.1155/2010/137201.
[63] "DeepLearningECGs - Databricks." https://databricks.com/notebooks/iot-medical/deep-learning.htm (accessed Sep. 09, 2021).
[64] Graohql, "GitHub: DataLoader ." https://github.com/graphql/dataloader (accessed Sep. 09, 2021).
[65] A. Pérez and E. Berjano, "Análisis, diseño y desarrollo de 'shields' de Arduino para procesamiento de señales fisiológicas," Universidad Politécnica de Valencia, Valencia, 2016.
[66] J. Brownlee, "What is the Difference Between a Parameter and a Hyperparameter?," Jul. 26, 2017. https://machinelearningmastery.com/difference-between-a-parameter-and-a-hyperparameter/ (accessed Sep. 11, 2021).
[67] J. Brownlee, "How to Choose an Activation Function for Deep Learning," Jan. 22, 2021. https://machinelearningmastery.com/choose-an-activation-function-for-deep-learning/ (accessed Sep. 11, 2021).
[68] Programador.dic, "Análisis del resumen del optimizador del método de optimización [TensorFlow] (SGD, Adagrad, Adadelta, Adam, Adamax, Nadam) ," Dec. 19, 2017. https://programmerclick.com/article/2432913113/ (accessed Sep. 11, 2021).
[69] D. Mwiti, "Keras Loss Functions: Everything You Need To Know - neptune.ai," Jul. 20, 2021. https://neptune.ai/blog/keras-loss-functions (accessed Sep. 11, 2021).
[70] X. Jin and J. de Lope, "Seguimiento ocular para el análisis del comportamiento mediante ANN," Universidad Politécnica de Madrid, Madrid, 20202.
[71] F. Dominguez, U. Kühl, B. Pieske, P. Garcia-Pavia, and C. Tschöpe, "Update on Myocarditis and Inflammatory Cardiomyopathy: Reemergence of Endomyocardial Biopsy," *Rev. Española Cardiol. (English Ed.*, vol. 69, no. 2, pp. 178–187, Feb. 2016, doi: 10.1016/J.REC.2015.10.015.
[72] UNSAM, "Tutorial: Programación en MATLAB." Accessed: Sep. 11, 2021. [Online]. Available: http://www.unsam.edu.ar/escuelas/ciencia/alumnos/Tutorial_Matlab_TDI.pdf.
[73] J. Rubin, S. Parvaneh, A. Rahman, B. Conroy, and S. Babaeizadeh, "Densely connected convolutional networks and signal quality analysis to detect atrial fibrillation using short single-lead ECG recordings," *Comput. Cardiol. (2010).*, vol. 44, pp. 1–4, 2017, doi: 10.22489/CinC.2017.160-246.

Annexes

Annex 1: Code on Python to Convert the WFDB in xlsx files

```
a= list(range(0,5000, 40))
signalsprecordiales=[]
for i in X:
  #signalspre= np.delete(i, (0,1,2,3,4,5), axis=1)
  signalspre=i[a]
  signalsprecordiales.append(signalspre)
  print(signalspre[1])
  #print(shape(signalspre[1]))
print('done')
cont=0 # 1
s=signalsprecordiales[0:1]
for signalspre in signalsprecordiales:
  data = {'v1': signalspre[:, 0],'v2': signalspre[:, 1],'v3': signa
lspre[:, 2],'v4': signalspre[:, 3],'v5': signalspre[:, 4],'v6': sig
nalspre[:, 5]}
 df = pd.DataFrame(data, columns = ['v1','v2','v3','v4','v5','v6'])
  name=lst[cont]
  writer =str(name)+str(cont) +'.xlsx'
  df.to_excel(writer, index=False)
  cont = cont + 1
  print(cont)
print('done')
```

Annex 2: Code of LSTM NN

```
from wfdb import io, plot
from tqdm import tqdm_notebook as tqdm
import os
import math
import matplotlib.pyplot as plt
%matplotlib notebook
import keras
      from keras.models import Sequential
      from keras.layers import Dense
      from keras.layers import Dropout, Input
      from keras.layers import LSTM
      from keras.layers.cudnn_recurrent import CuDNNLSTM
      from keras.callbacks import ModelCheckpoint
from sklearn.utils import shuffle
from sklearn.metrics import confusion_matrix
import numpy as np
import pandas as pd
import time

def make_model(input_shape, output_dim, lstm_layer, dropout=0.2):
    model = Sequential()
    model.add(lstm_layer(256, return_sequences=True, input_shape=in
put_shape, batch_size=None))
    model.add(Dropout(dropout))
    model.add(lstm_layer(128, return_sequences=True))
    model.add(Dropout(dropout))
```

```
    model.add(LSTM(64))
    model.add(Dropout(dropout))
    model.add(Dense(output_dim, activation='softmax'))
    model.compile(loss= 'categorical_crossentropy', optimizer='adam
', metrics=['accuracy'])
    return model

fractions = 1-trainY.sum(axis=0)/len(trainY)
weights = fractions[trainY.argmax(axis=1)]

model = make_model((trainX.shape[1], trainX.shape[2]), trainY.shape
[-1], LSTM)

dnn= model.fit(trainX, trainY, epochs=12, batch_size=500, sample_we
ight=weights, validation_data=(testX, testY))
```

Annex 3: Code of ResNet34 NN

```
!pip install fastai --upgrade -q
from fastai import *
from fastai.vision import *
from fastai.vision.data import *
from fastai.data.all import *
from fastai.vision.all import *
from fastai.metrics import error_rate
from fastai.vision.data import ImageDataLoaders

fields = DataBlock(blocks=(ImageBlock, CategoryBlock), get_items=ge
t_image_files,get_y=parent_label, splitter=RandomSplitter(),item_tf
ms = Resize(224))

dls=fields.dataloaders(path,bs=batch_size)

learn = cnn_learner(dls, models.resnet34, lr=0.001, metrics=[accura
cy, error_rate])
```

Annex 4: Code on Arduino to Acquire the Signal

```
void setup() {
  Serial.begin(9600);
}
void loop() {
  int V1 = analogRead(A0);
  int V2 = analogRead(A1);
  int V3 = analogRead(A2);
  int V4 = analogRead(A3);
  int V5 = analogRead(A4);
  int V6 = analogRead(A5);
  Serial.print("V1:"); Serial.print(V1); Serial.print(" ");
  Serial.print("V2:"); Serial.print(V2); Serial.print(" ");
  Serial.print("V3:"); Serial.print(V3); Serial.print(" ");
  Serial.print("V4:"); Serial.print(V4); Serial.print(" ");
  Serial.print("V5:"); Serial.print(V5); Serial.print(" ");
  Serial.print("V6:"); Serial.print(V6); Serial.print(" ");
  Serial.println();
  delay(1);  }
```

Annex 5: Code on MATLAB to Filter the Signal

```
%% SIGNAL
filename= 'ARDUINOSIGNAL.xlsx';
t = (0:0.002:9.998).';
duracion_muestreo = 10;  %seconds
fs = 5000;                %sampling rate
numero_muestras = duracion_muestreo*fs;%number of samples

V1 = xlsread(filename,'A:A'); V2 = xlsread(filename,'B:B');
V3 = xlsread(filename,'C:C'); V4 = xlsread(filename,'D:D');
V5 = xlsread(filename,'E:E'); V6 = xlsread(filename,'F:F');

%% Signal inversion and amplification
media1=median(V1); V1inv=abs(-V1+media1).*(300/1024);
media2=median(V2); V2inv=abs(-V2+media2).*(300/1024);
media3=median(V3); V3inv=abs(-V3+media3).*(300/1024);
media4=median(V4); V4inv=abs(-V4+media4).*(300/1024);
media5=median(V5); V5inv=abs(-V5+media5).*(300/1024);
media6=median(V6); V6inv=abs(-V6+media6).*(300/1024);

%% SIGNAL FILTERING: BANDPASS FILTER
n=4;             %filter order
fcutlow=0.05;    %low cut frequency in Hz
fcuthigh=100;    %high cut frequency in Hz
[d, c] = butter(n,[fcutlow,fcuthigh]/(fs/2),'bandpass');

F1V1=filtfilt(d,c,V1inv);
F1V2=filtfilt(d,c,V2inv);
F1V3=filtfilt(d,c,V3inv);
F1V4=filtfilt(d,c,V4inv);
F1V5=filtfilt(d,c,V5inv);
F1V6=filtfilt(d,c,V6inv);

%% SIGNAL FILTERING: BAND REJECTION FILTER
fcn=60; Wo=fcn/(fs/2); BW=Wo/10; [b, a]=iirnotch(Wo,BW);

F2V1=(filtfilt(b,a,F1V1));
F2V2=(filtfilt(b,a,F1V2));
F2V3=(filtfilt(b,a,F1V3));
F2V4=(filtfilt(b,a,F1V4));
F2V5=(filtfilt(b,a,F1V5));
F2V6=(filtfilt(b,a,F1V6));

%% Original Signal
ekg=V1+V2+V3+V4+V5+V6;
figure ('Name', 'Original ECG Signal')
plot(t,ekg,'b');
title('ECG Signal'); xlabel('Samples'); ylabel('f(Samples)');
legend('ECG=V1+V2+V3+V4+V5+V6');

%% Filtered Signal
ekg2=F2V1+F2V2+F2V3+F2V4+F2V5+F2V6;
figure ('Name', 'Filtered ECG signal')
plot(t,ekg2,'b');
title('ECG Signal'); xlabel('Samples'); ylabel('f(Samples)');
legend('ECG=V1+V2+V3+V4+V5+V6');
```

Annex 6: Images of the Signal Processing of Patient01

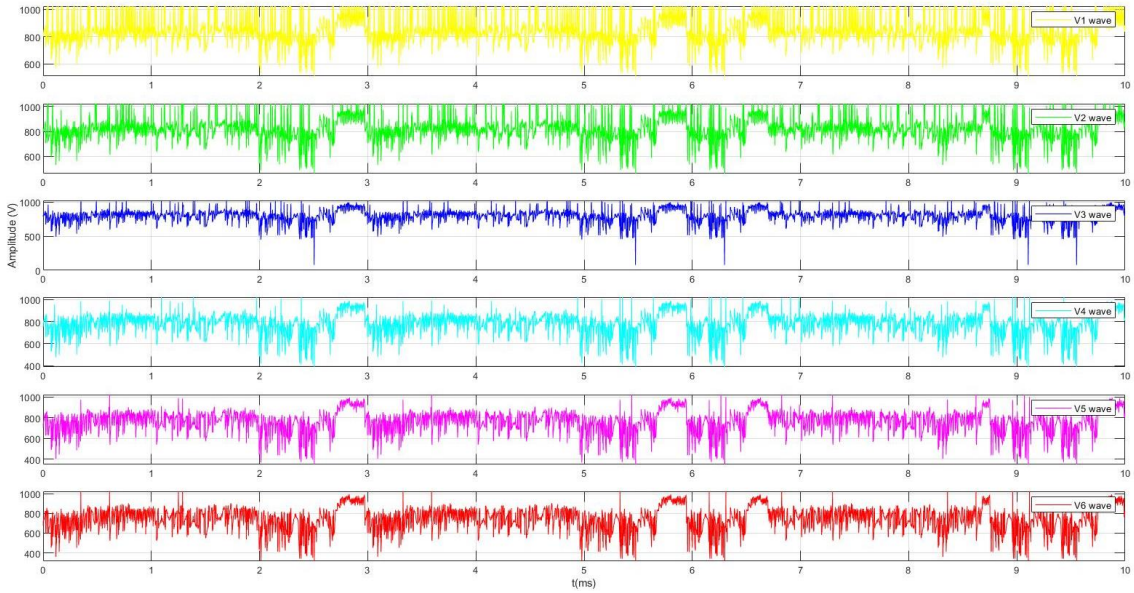

Figure 32. Graph at MATLAB of the ECG Precordial Waves of Patient01 obtained in Arduino along 10 seconds (x-axis) for the Amplitude (y-axis).

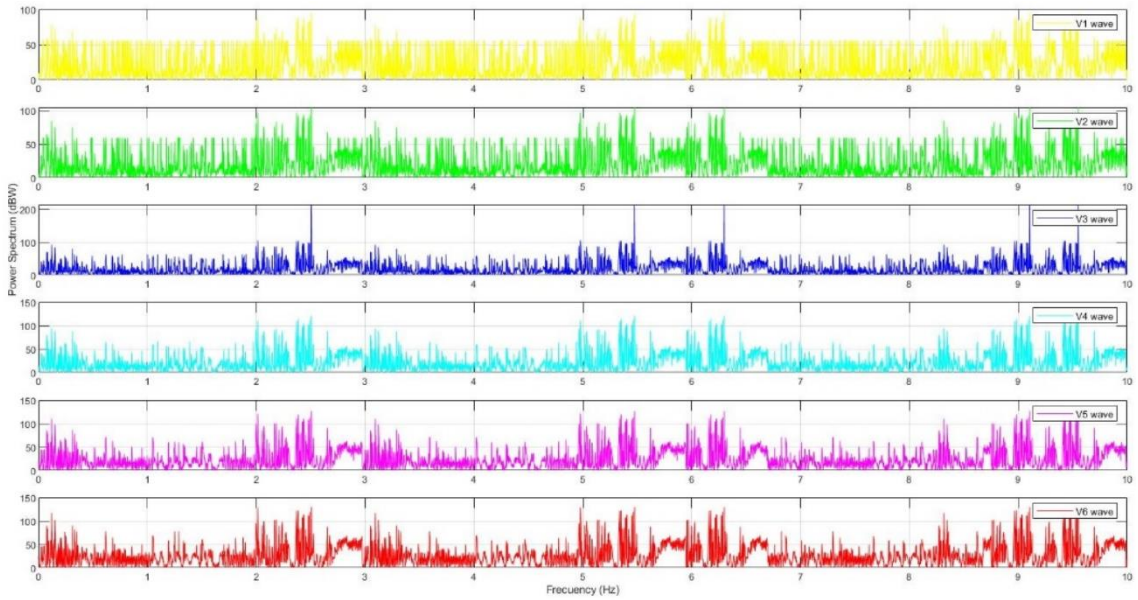

Figure 33. Plot at MATLAB of Patient01's ECG Precordial Waves after inversion and amplification of the signal by a factor of 60.

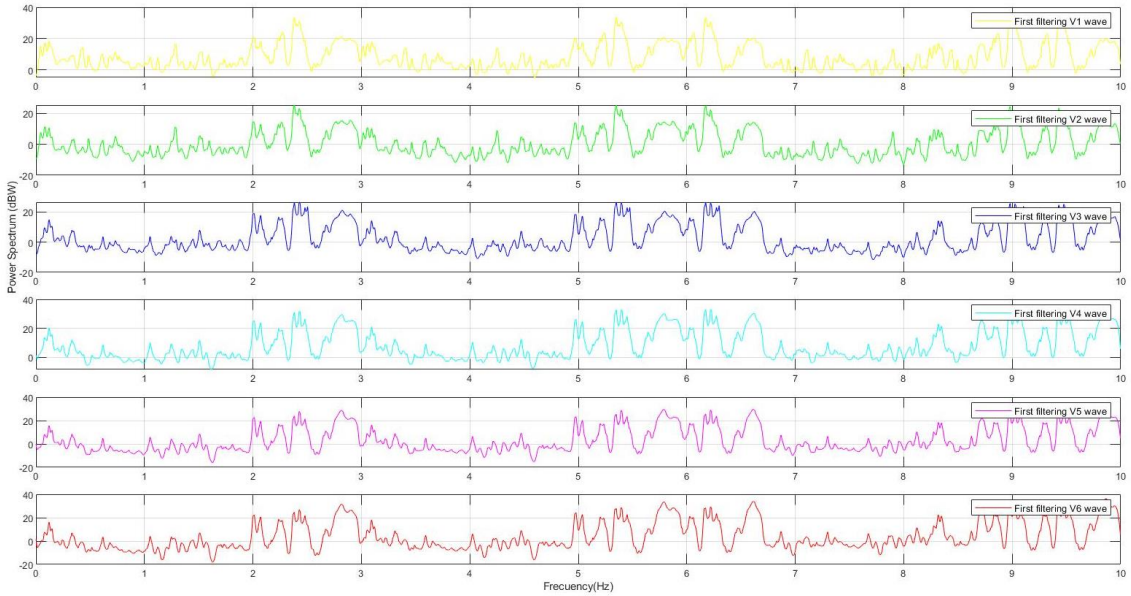

Figure 34. Plot at MATLAB of Patient01's ECG Precordial Waves applying a band-pass filter with a cut low of 0.05 and a cut high of 100 Hz.

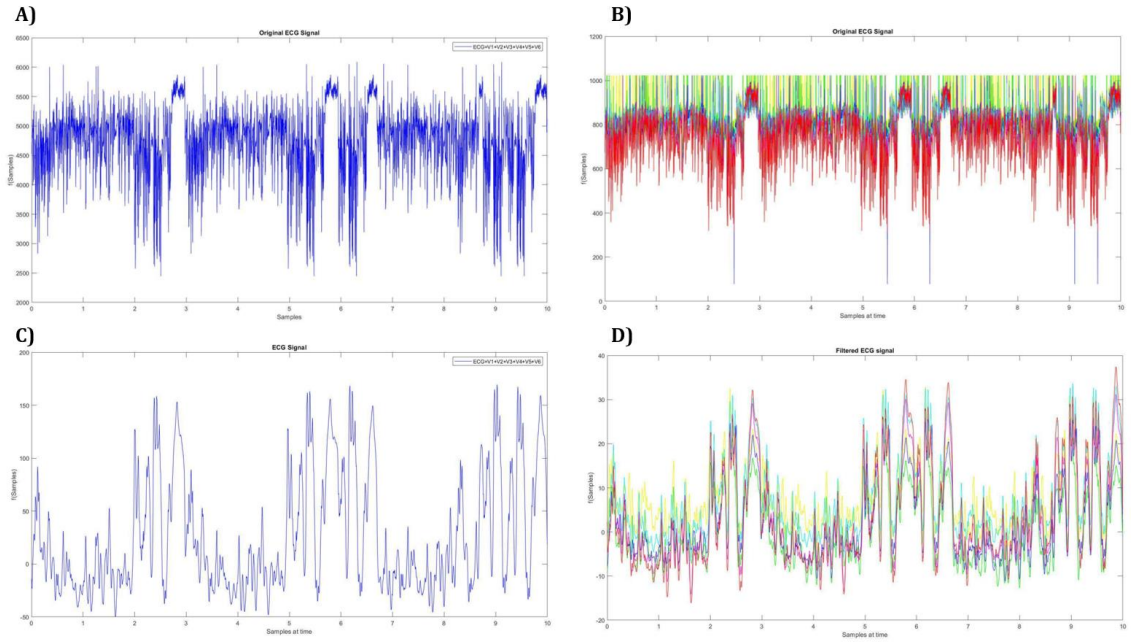

Figure 35. Graph at MATLAB of the Patient01 signals: A) 6-lead combined signal obtained in Arduino, B) 6 individual leads signals obtained in Arduino, C) 6-lead combined signal already filtered, B) 6 individual leads signals already filtered, C) 6 individual leads signals already filtered, C) 6 individual leads signals already filtered.

Annex 7: Images of the Signal Processing of Patient02

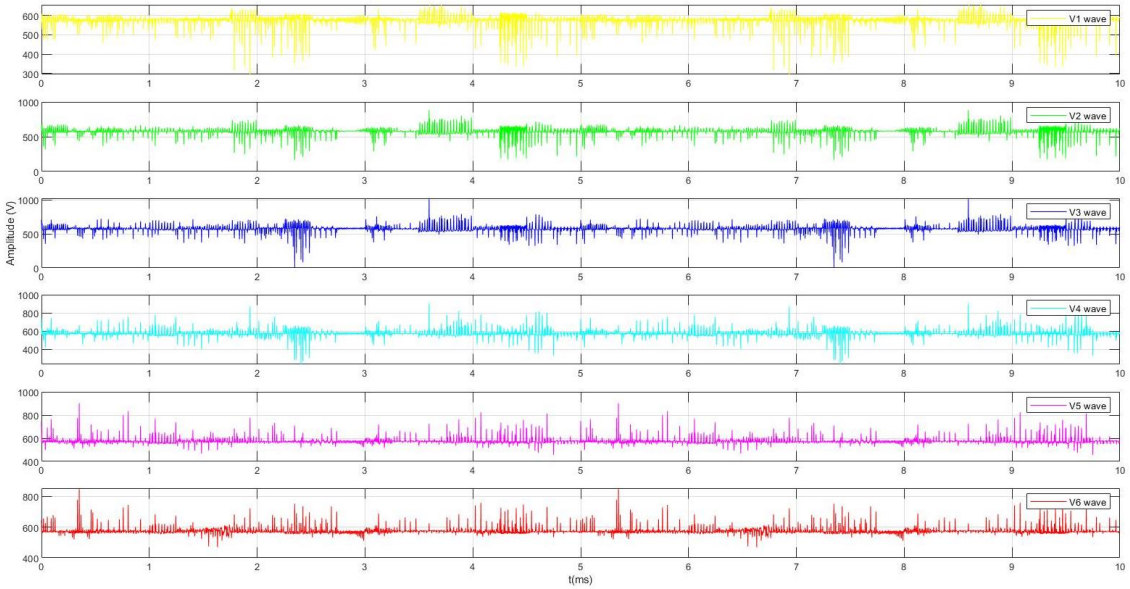

Figure 36. Graph at MATLAB of the ECG Precordial Waves of Patient02 obtained in Arduino along 10 seconds (x-axis) for the Amplitude (y-axis).

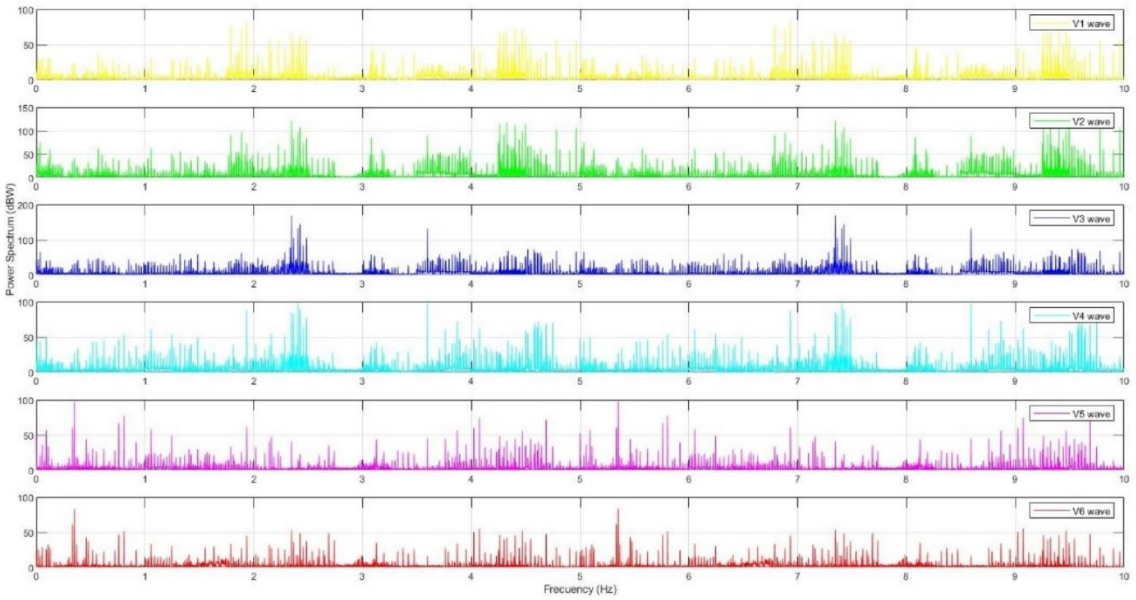

Figure 37. Plot at MATLAB of Patient02's ECG Precordial Waves after inversion and amplification of the signal by a factor of 60.

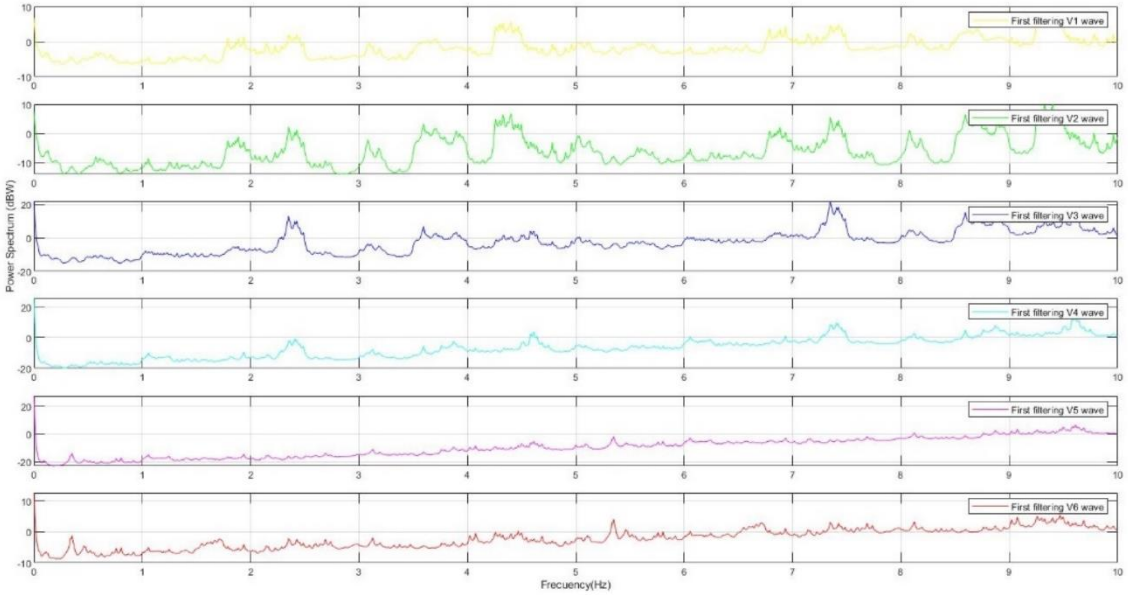

Figure 38. Plot at MATLAB of Patient01's ECG Precordial Waves applying a band-pass filter with a cut low of 0.05 and a cut high of 100 Hz.

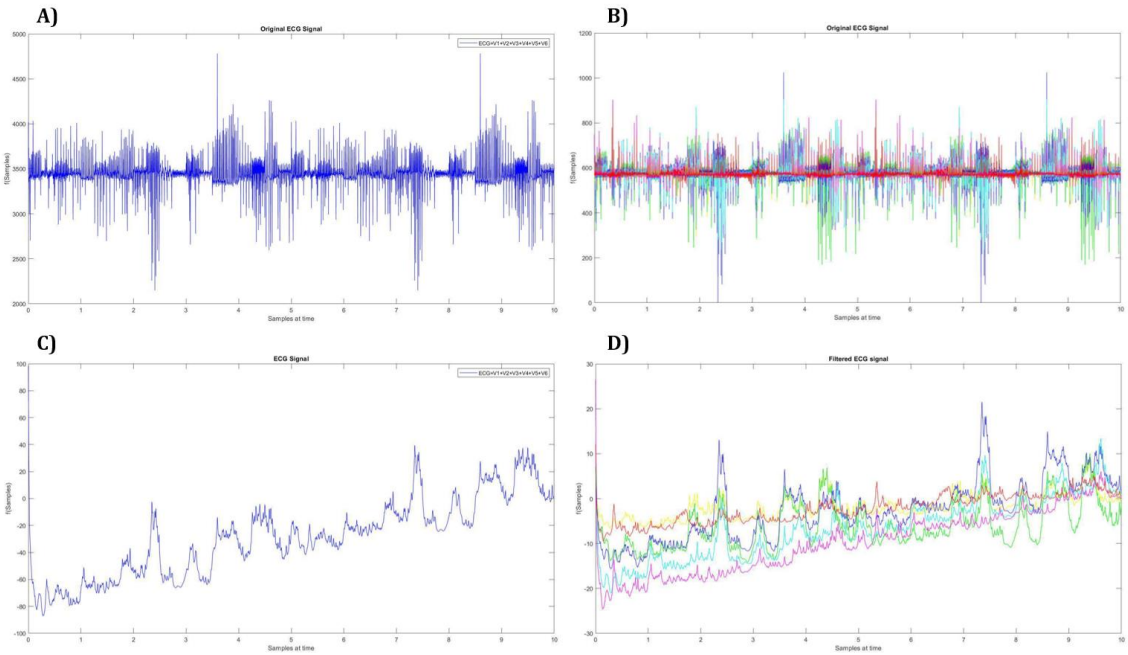

Figure 39. Graph at MATLAB of the Patient02 signals: A) 6-lead combined signal obtained in Arduino, B) 6 individual leads signals obtained in Arduino, C) 6-lead combined signal already filtered, B) 6 individual leads signals already filtered, C) 6 individual leads signals already filtered, C) 6 individual leads signals already filtered.